

THE MESON PRODUCTION IN PROTON-PROTON COLLISIONS IN NEXT-TO-LEADING ORDER AND INFRARED RENORMALONS

A. I. Ahmadov^{1,2} * and R. M. Burjaliyev²

¹ *The Abdus Salam International Centre for Theoretical Physics*

Strada Costiera 11, 34014, Trieste, Italy and

² *Department of Theoretical Physics, Baku State University*

Z. Khalilov Street 23, AZ-1148, Baku, Azerbaijan

Abstract

In this article, we investigate the next-to-leading order contribution of the higher-twist Feynman diagrams to the large- p_T inclusive pion production cross section in proton-proton collisions and present the general formulae for the higher-twist differential cross sections in the case of the running coupling and frozen coupling approaches. We compared the resummed next-to-leading order higher-twist cross sections with the ones obtained in the framework of the frozen coupling approach and leading-twist cross section. The structure of infrared renormalon singularities of the higher twist subprocess cross section and its resummed expression (the Borel sum) are found. It is shown that the resummed result depends on the choice of the meson wave functions used in the calculations. We discuss the phenomenological consequences of possible higher-twist contributions to the meson production in proton-proton collisions in next-to-leading order at RHIC.

PACS numbers: 12.38.-t, 13.60.Le, 13.87.Fh, 14.40.Aq,

Keywords: higher-twist, pion wave function, infrared renormalons

* ahmadovazar@yahoo.com

I. INTRODUCTION

The large-order behavior of a perturbative expansion in gauge theories is inevitably dominated by the factorial growth of renormalon diagrams [1-4]. In the case of quantum chromodynamics (QCD), the coefficients of perturbative expansions in the QCD coupling α_s can increase dramatically even at low orders. This fact, together with the apparent freedom in the choice of renormalization scheme and renormalization scales, limits the predictive power of perturbative calculations, even in applications involving large momentum transfers, where α_s is effectively small.

A number of theoretical approaches have been developed to reorganize the perturbative expansions in an effort to improve the predictability of the perturbative QCD (pQCD). For example, optimized scale and scheme choices have been proposed, such as the method of effective charges (ECH) [5], the principle of minimal sensitivity (PMS) [6], and the Brodsky-Lepage-Mackenzie (BLM) scale-setting prescription [7] and its generalizations [8-20]. In Ref.[4], the resummation of the formally divergent renormalon series and the parametrization of related higher-twist power-suppressed contributions has been given.

In general, a factorially divergent renormalon series arises when one integrates over the logarithmically running coupling $\alpha_s(k^2)$ in a loop diagram. Such contributions do not occur in conformally invariant theories which have a constant coupling. Of course, in the physical theory, the QCD coupling does run.

Among the fundamental predictions of QCD are asymptotic scaling laws for large-angle exclusive processes [21-28]. QCD counting rules were formalized in Refs.[22,23]. These reactions probe hadronic constituents at large relative momenta, or equivalently, the hadronic wave function at short distances. In particular, the meson wave function determines the leading higher-twist contribution to meson production at high p_T .

The hadronic wave functions in terms of quark and gluon degrees of freedom play an important role in the quantum chromodynamics predictions for hadronic processes. In the perturbative QCD theory, the hadronic distribution amplitudes and structure functions which enter exclusive and inclusive processes via the factorization theorems at high momentum transfers can be determined by the hadronic wave functions, and therefore they are the underlying links between hadronic phenomena in QCD at large (nonperturbative) and small distances (perturbative). If the hadronic wave functions were accurately known, then we

could calculate the hadronic distribution amplitude and structure functions for exclusive and inclusive processes in QCD.

The study of hadron production at large transverse momenta in hadronic interactions is a valuable testing ground of the perturbative regime of QCD, providing information on both the parton distribution functions (PDFs) in the proton, and the parton-to-hadron fragmentation functions (FFs)[29].

The frozen coupling constant approach can be applied for investigation, not only for exclusive processes, but also for the calculation of higher-twist contributions to some inclusive processes, for example as large $-p_T$ meson photoproduction [30], two-jet+meson production in the electron-positron annihilation [31]. In the frozen coupling constant approach was used Refs.[30,31] for calculation of integrals, such as

$$I \sim \int \frac{\alpha_s(\hat{Q}^2)\Phi(x, \hat{Q}^2)}{1-x} dx \quad (1.1)$$

According to Ref.[7], in pQCD calculations, the argument \hat{Q}^2 of the running coupling constant should be taken equal to the square of the momentum transfer of a hard gluon in a corresponding Feynman diagram, in both the renormalization and factorization scale. But defined in this way, $\alpha_s(\hat{Q}^2)$ suffers from infrared singularities. For example in Ref.[32], \hat{Q}^2 equals to $(x_1 - 1)\hat{u}$ and $-x_1\hat{t}$, where \hat{u} , \hat{t} are the subprocess's Mandelstam invariants. Therefore, in the soft regions $x_1 \rightarrow 0$, $x_2 \rightarrow 0$, the integrals in (1.1) diverge and we need some regularization methods of $\alpha_s(Q^2)$ in these regions for their calculation. In Ref.[33], the authors investigated the phenomenology of infrared renormalons in inclusive processes. The dispersive approach has been devised to extend properly modified perturbation theory calculations towards the low-energy region [34]. Connections between power corrections for the three Deep Inelastic Scattering sum rules have also been explored in Ref.[35].

Investigation of the infrared renormalon effects in various inclusive and exclusive processes is one of the most important and interesting problems in the perturbative QCD. It is known that infrared renormalons are responsible for factorial growth of coefficients in perturbative series for the physical quantities. But, these divergent series can be resummed by means of the Borel transformation [1] and the principal value prescription [36], and effects of infrared renormalons can be taken into account by a scale-setting procedure $\alpha_s(Q^2) \rightarrow \alpha_s(\exp(f(Q^2))Q^2)$ at the one-loop order results. Technically, all-order resummation of infrared renormalons corresponds to the calculation of the one-loop Feynman

diagrams with the running coupling constant $\alpha_s(-k^2)$ at the vertices or, alternatively, to calculation of the same diagrams with nonzero gluon mass. Studies of infrared renormalon problems have also opened new prospects for evaluation of power-suppressed corrections to processes characteristics [37]. Power corrections can also be obtained by means of the Landau-pole free expression for the QCD coupling constant. The most simple and elaborated variant of the dispersive approach, the Shirkov and Solovtsov analytic perturbation theory, was formulated in Ref.[38].

By taking these points into account, it may be argued that the analysis of the next-to-leading order higher-twist effects on the dependence of the pion wave function in pion production at proton-proton collisions by the running coupling approach, are significant from both theoretical and experimental[39] points of view.

In this work we apply the running coupling approach[40] in order to compute the effects of the infrared renormalons on the meson production in proton-proton collisions in next-to-leading order. This approach was also employed previously[41,42] to calculate the inclusive meson production in proton-proton and photon-photon collisions. The running coupling method in next-to-leading order pion and kaon electromagnetic form factor was computed in [43].

As we know, power-suppressed contributions to exclusive processes in QCD, which are commonly referred to as higher-twist corrections. The higher-twist approximation describes the multiple scattering of a parton as power corrections to the leading-twist cross section.

We will show that higher-twist terms contribute substantially to the inclusive meson cross section at moderate transverse momenta. In addition, we shall demonstrate that higher-twist reactions necessarily dominate in the kinematic limit where the transverse momentum approaches the phase-space boundary.

A precise measurement of the inclusive charged pion production cross section at $\sqrt{s} = 62.4 \text{ GeV}$ and $\sqrt{s} = 200 \text{ GeV}$ is important for the proton-proton collisions program at the Relativistic Heavy Ion Collider (RHIC) at the Brookhaven National Laboratory. Another important aspect of this study is the choice of the meson model wave functions. In this respect, the contribution of the higher-twist Feynman diagrams to a pion production cross section in proton-proton collisions is been computed by using various pion wave functions. Also, higher-twist contributions which are calculated by the running coupling constant and frozen coupling constant approaches are been estimated and compared to each other. Within

this context, this paper is organized as follows: In Sec.II, we provide formulas for the calculation of the contribution of the high twist diagrams. In Sec. III we present formulas and an analysis of the next-to-leading order higher-twist effects on the dependence of the pion wave function by the running coupling constant approach. In Sec. IV, we provide formulas for the calculation of the contribution of the leading-twist diagrams. In Sec. V, we give the numerical results for the cross section and discuss the dependence of the cross section on the pion wave functions. We present our conclusions in Sec. VI.

II. CONTRIBUTION OF THE HIGH TWIST DIAGRAMS

The higher-twist Feynman diagrams, which describe the subprocess $q_1 + \bar{q}_2 \rightarrow \pi^+(\pi^-) + \gamma$ for the pion production in the proton-proton collision are shown in Fig.1. In the higher-twist diagrams, the pion of a proton quark is directly observed. Their $1/Q^2$ power suppression is caused by a hard gluon exchange between pion constituents. The amplitude for this subprocess can be found by means of the Brodsky-Lepage formula [27]:

$$M(\hat{s}, \hat{t}) = \int_0^1 dx_1 \int_0^1 dx_2 \delta(1 - x_1 - x_2) \Phi_\pi(x_1, x_2, Q^2) T_H(\hat{s}, \hat{t}; x_1, x_2). \quad (2.1)$$

In Eq.(2.1), T_H is the sum of the graphs contributing to the hard-scattering part of the subprocess. The hard-scattering part for the subprocess under consideration is $q_1 + \bar{q}_2 \rightarrow (q_1 \bar{q}_2) + \gamma$, where a quark and antiquark form a pseudoscalar, color-singlet state $(q_1 \bar{q}_2)$. Here $\Phi(x_1, x_2, Q^2)$ is the pion wave function, i.e., the probability amplitude for finding the valence $q_1 \bar{q}_2$ Fock state in the meson carry fractions x_1 and x_2 , $x_1 + x_2 = 1$. Remarkably, this factorization is gauge invariant and only requires that the momentum transfers in T_H be large compared to the intrinsic mass scales of QCD. Since the distribution amplitude and the hard-scattering amplitude are defined without reference to the perturbation theory, the factorization is valid to leading order in $1/Q$, independent of the convergence of perturbative expansions.

The hard-scattering amplitude T_H can be calculated in perturbation theory and represented as a series in the QCD running coupling constant $\alpha_s(Q^2)$. The function Φ is intrinsically nonperturbative, but its evolution can be calculated perturbatively. In our calculation, we have neglected the pion and the proton masses. Turning to extracting the contributions of the higher-twist subprocesses, there are many kinds of leading-twist subprocesses in pp

collisions as the background of the higher-twist subprocess $q_1 + q_2 \rightarrow \pi^+$ (or π^-) + γ , such as $q + \bar{q} \rightarrow \gamma + g(g \rightarrow \pi^+(\pi^-))$, $q + g \rightarrow \gamma + q(q \rightarrow \pi^+(\pi^-))$, $\bar{q} + g \rightarrow \gamma + \bar{q}g(\bar{q} \rightarrow \pi^+(\pi^-))$ etc. The contributions from these leading-twist subprocesses strongly depend on some phenomenological factors, for example, quark and gluon distribution functions in the proton and fragmentation functions of various constituents, etc. Most of these factors have not been well determined, neither theoretically nor experimentally. Thus they cause very large uncertainty in the computation of the cross section of process $pp \rightarrow \pi^+$ (or π^-) + γ + X . In general, the magnitude of this uncertainty is much larger than the sum of all the higher-twist contributions, so it is very difficult to extract the higher-twist contributions.

The production of a hadron at large transverse momentum, p_T , in a hadronic collisions is conventionally analyzed within the framework of perturbative QCD by convoluting the leading-twist $2 \rightarrow 2$ hard subprocess cross sections with evolved structure and fragmentation functions. The most important discriminant of the twist of a perturbative QCD subprocess in a hard hadronic collision is the scaling of the inclusive invariant cross section [22-25,44],

$$\sigma^{inv} \equiv E \frac{d\sigma}{d^3p}(AB \rightarrow CX) = \frac{F(x_{p_T}, \vartheta)}{p_T^n} \quad (2.2)$$

at fixed $x_T = 2p_T/\sqrt{s}$ and center-of-mass angle ϑ . As we know in the original parton model [45] the power fall-off is simply $n = 4$ since the $2 \rightarrow 2$ subprocess amplitude for point-like partons is scale invariant, and there is no dimensional parameter as in a conformal theory. The detected hadron C can be produced directly in the hard subprocess reaction as in an exclusive reaction, then such direct higher-twist processes can give a significant contribution since there is no suppression from jet fragmentation at large momentum fraction carried by the hadron, z , and the trigger hadron is produced without any waste of energy[44].

The Mandelstam invariant variables for subprocesses $q_1 + \bar{q}_2 \rightarrow \pi^+(\pi^-) + \gamma$ are defined as

$$\hat{s} = (p_1 + p_2)^2, \quad \hat{t} = (p_1 - p_\pi)^2, \quad \hat{u} = (p_1 - p_\gamma)^2. \quad (2.3)$$

In our calculation, we have also neglected the quark masses. We have aimed to calculate the pion production cross section and to fix the differences due to the use of various pion model functions. We have used five different wave functions: the asymptotic wave function (ASY), the Chernyak-Zhitnitsky wave function [28,46], the CLEO wave function [47], the Braun-Filyanov pion wave functions [48] and the Bakulev-Mikhailov-Stefanis pion wave

function [49]. It should be noted that the wave functions of pions also are developed in Refs.[50-52] by the Dubna group:

$$\begin{aligned}
\Phi_{CZ}(x, \mu_0^2) &= \Phi_{asy}(x) \left[C_0^{3/2}(2x-1) + \frac{2}{3}C_2^{3/2}(2x-1) \right], \\
\Phi_{CLEO}(x, \mu_0^2) &= \Phi_{asy}(x) \left[C_0^{3/2}(2x-1) + 0.27C_2^{3/2}(2x-1) - 0.22C_4^{3/2}(2x-1) \right], \\
\Phi_{BF}(x, \mu_0^2) &= \Phi_{asy}(x) \left[C_0^{3/2}(2x-1) + 0.44C_2^{3/2}(2x-1) + 0.25C_4^{3/2}(2x-1) \right], \\
\Phi_{BMS}(x, \mu_0^2) &= \Phi_{asy}(x) \left[C_0^{3/2}(2x-1) + 0.188C_2^{3/2}(2x-1) - 0.13C_4^{3/2}(2x-1) \right], \quad (2.4) \\
\Phi_{asy}(x) &= \sqrt{3}f_\pi x(1-x), \\
C_0^{3/2}(2x-1) &= 1, \quad C_2^{3/2}(2x-1) = \frac{3}{2}(5(2x-1)^2 - 1), \\
C_4^{3/2}(2x-1) &= \frac{15}{8}(21(2x-1)^4 - 14(2x-1)^2 + 1),
\end{aligned}$$

where $f_\pi = 0.923 GeV$ is the pion decay constant. Here, we have denoted by $x \equiv x_1$, the longitudinal fractional momentum carried by the quark within the meson. Then, $x_2 = 1 - x$ and $x_1 - x_2 = 2x - 1$. The pion wave function is symmetric under the replacement $x_1 - x_2 \leftrightarrow x_2 - x_1$.

Several important nonperturbative tools have been developed which allow specific predictions for the hadronic wave functions directly from theory and experiments. The QCD sum-rule technique and lattice gauge theory provide constraints on the moments of the hadronic distribution amplitude. However, the correct pion wave function is still an open problem in QCD. It is known that the pion wave function can be expanded over the eigenfunctions of the one-loop Brodsky-Lepage equation, *i.e.*, in terms of the Gegenbauer polynomials $\{C_n^{3/2}(2x-1)\}$:

$$\Phi_\pi(x, Q^2) = \Phi_{asy}(x) \left[1 + \sum_{n=2,4..}^{\infty} a_n(Q^2) C_n^{3/2}(2x-1) \right]. \quad (2.5)$$

The evolution of the wave function on the factorization scale Q^2 is governed by the functions $a_n(Q^2)$,

$$\begin{aligned}
a_n(Q^2) &= a_n(\mu_0^2) \left[\frac{\alpha_s(Q^2)}{\alpha_s(\mu_0^2)} \right]^{\gamma_n/\beta_0}, \quad (2.6) \\
\frac{\gamma_2}{\beta_0} &= \frac{50}{81}, \quad \frac{\gamma_4}{\beta_0} = \frac{364}{405}, \quad n_f = 3.
\end{aligned}$$

In Eq.(2.6), $\{\gamma_n\}$ are anomalous dimensions defined by the expression,

$$\gamma_n = C_F \left[1 - \frac{2}{(n+1)(n+2)} + 4 \sum_{j=2}^{n+1} \frac{1}{j} \right]. \quad (2.7)$$

The constants $a_n(\mu_0^2) = a_n^0$ are input parameters that form the shape of the wave functions and which can be extracted from experimental data or obtained from the nonperturbative QCD computations at the normalization point μ_0^2 . The QCD coupling constant $\alpha_s(Q^2)$ at the one-loop approximation is given by the expression,

$$\alpha_s(Q^2) = \frac{4\pi}{\beta_0 \ln(Q^2/\Lambda^2)}. \quad (2.8)$$

Here, Λ is the fundamental QCD scale parameter, β_0 is the QCD beta function one-loop coefficient, respectively,

$$\beta_0 = 11 - \frac{2}{3}n_f.$$

The cross section for the higher-twist subprocess $q_1 \bar{q}_2 \rightarrow \pi^+(\pi^-)\gamma$ is given by the expression

$$\frac{d\sigma}{d\hat{t}}(\hat{s}, \hat{t}, \hat{u}) = \frac{8\pi^2 \alpha_E C_F}{27} \frac{[D(\hat{t}, \hat{u})]^2}{\hat{s}^3} \left[\frac{1}{\hat{u}^2} + \frac{1}{\hat{t}^2} \right], \quad (2.9)$$

where

$$D(\hat{t}, \hat{u}) = e_1 \hat{t} \int_0^1 dx \left[\frac{\alpha_s(\hat{Q}_1^2) \Phi_\pi(x, \hat{Q}_1^2)}{1-x} \right] + e_2 \hat{u} \int_0^1 dx \left[\frac{\alpha_s(\hat{Q}_2^2) \Phi_\pi(x, \hat{Q}_2^2)}{1-x} \right]. \quad (2.10)$$

Here $\hat{Q}_1^2 = (x_1 - 1)\hat{u}$, and $\hat{Q}_2^2 = -x_1\hat{t}$, represent the momentum squared carried by the hard gluon in Fig.1, $e_1(e_2)$ is the charge of $q_1(\bar{q}_2)$ and $C_F = \frac{4}{3}$. The higher-twist contribution to the large- p_T pion production cross section in the process $pp \rightarrow \pi^+(\pi^-) + \gamma + X$ is [53]:

$$\Sigma_M^{HT} \equiv E \frac{d\sigma}{d^3p} = \int_0^1 \int_0^1 dx_1 dx_2 G_{q_1/h_1}(x_1) G_{q_2/h_2}(x_2) \frac{\hat{s}}{\pi} \frac{d\sigma}{d\hat{t}}(q\bar{q} \rightarrow \pi\gamma) \delta(\hat{s} + \hat{t} + \hat{u}). \quad (2.11)$$

$$\pi E \frac{d\sigma}{d^3p} = \frac{d\sigma}{dy dp_T^2},$$

$$\hat{s} = x_1 x_2 s,$$

$$\hat{t} = x_1 t,$$

$$\hat{u} = x_2 u, \quad (2.12)$$

$$t = -m_T \sqrt{s} e^{-y} = -p_T \sqrt{s} e^{-y},$$

$$u = -m_T \sqrt{s} e^y = -p_T \sqrt{s} e^y,$$

$$x_1 = -\frac{x_2 u}{x_2 s + t} = \frac{x_2 p_T \sqrt{s} e^y}{x_2 s - p_T \sqrt{s} e^{-y}},$$

$$x_2 = -\frac{x_1 t}{x_1 s + u} = \frac{x_1 p_T \sqrt{s} e^{-y}}{x_1 s - p_T \sqrt{s} e^y},$$

where m_T – is the transverse mass of pion, which is given by

$$m_T^2 = m^2 + p_T^2$$

Let us first consider the frozen coupling approach. In this approach, we take the four-momentum square $\hat{Q}_{1,2}^2$ of the hard gluon to be equal the pion's transverse momentum square $\hat{Q}_{1,2}^2 = p_T^2$. In this case, the QCD coupling constant α_s in the integral (2.10) does not depend on the integration variable. After this substitution calculation of integral (2.10) becomes easy. Hence, the effective cross section obtained after substitution of the integral (2.10) into the expression (2.9) is referred as the frozen coupling effective cross section. We will denote the higher-twist cross section obtained using the frozen coupling constant approximation by $(\Sigma_\pi^{HT})^0$.

We have extracted the following higher-twist subprocesses contributing to the two covariant cross sections in Eq.(2.11)

$$\frac{d\sigma^1}{d\hat{t}}(u\bar{d} \rightarrow \pi^+\gamma), \quad \frac{d\sigma^2}{d\hat{t}}(\bar{d}u \rightarrow \pi^+\gamma), \quad \frac{d\sigma^3}{d\hat{t}}(\bar{u}d \rightarrow \pi^-\gamma), \quad \frac{d\sigma^4}{d\hat{t}}(d\bar{u} \rightarrow \pi^-\gamma). \quad (2.13)$$

By charge conjugation invariance, we also have

$$\frac{d\sigma^1}{d\hat{t}}(u\bar{d} \rightarrow \pi^+\gamma) = \frac{d\sigma^3}{d\hat{t}}(\bar{u}d \rightarrow \pi^-\gamma), \quad \text{and} \quad \frac{d\sigma^2}{d\hat{t}}(\bar{d}u \rightarrow \pi^+\gamma) = \frac{d\sigma^4}{d\hat{t}}(d\bar{u} \rightarrow \pi^-\gamma). \quad (2.14)$$

III. THE RUNNING COUPLING APPROACH AND HIGHER-TWIST MECHANISM

In this section, we shall calculate the integral (2.10) using the running coupling constant method and also discuss the problem of normalization of the higher-twist process cross section in the context of the same approach.

As is seen from (2.10), in general, one has to take into account not only the dependence of $\alpha(\hat{Q}_{1,2}^2)$ on the scale $\hat{Q}_{1,2}^2$, but also an evolution of $\Phi(x, \hat{Q}_{1,2}^2)$ with $\hat{Q}_{1,2}^2$. The meson wave function evolves in accordance with a Bethe-Salpeter-type equation. Therefore, it is worth noting that, the renormalization scale (argument of α_s) should be equal to $Q_1^2 = (x_1 - 1)\hat{u}$,

$Q_2^2 = -x_1 \hat{t}$, whereas the factorization scale [Q^2 in $\Phi_M(x, Q^2)$] is taken independent from x , we assume $Q^2 = p_T^2$. Such a approximation does not considerably change the numerical results, but the phenomenon considered in this article (effect of infrared renormalons) becomes transparent. The main problem in our investigation is the calculation of the integral in (2.10) by the running coupling constant approach. This integral in the framework of the running coupling approach takes the form

$$I(\mu_{R_0}^2) = \int_0^1 \frac{\alpha_s(\lambda \mu_{R_0}^2) \Phi_M(x, \mu_F^2) dx}{1-x}. \quad (3.1)$$

The $\alpha_s(\lambda \mu_{R_0}^2)$ has the infrared singularity at $x \rightarrow 1$, if $\lambda = 1 - x$ or $x \rightarrow 0$, if $\lambda = x$ and as a result integral (3.1) diverges (the pole associated with the denominator of the integrand is fictitious, because $\Phi_M \sim (1 - x)$, and therefore, the singularity of the integrand at $x = 1$ is caused only by $\alpha_s(\lambda \mu_{R_0}^2)$). For the regularization of the integral, we express the running coupling at scaling variable $\alpha_s(\lambda \mu_{R_0}^2)$ with the aid of the renormalization group equation in terms of the fixed one $\alpha_s(Q^2)$. The renormalization group equation for the running coupling $\alpha \equiv \alpha_s/\pi$ has the form [36]

$$\frac{\partial \alpha(\lambda Q^2)}{\partial \ln \lambda} \simeq -\frac{\beta_0}{4} [\alpha(\lambda Q^2)]^2 - \frac{\beta_1}{16} [\alpha(\lambda Q^2)]^3 \quad (3.2)$$

where

$$\beta_0 = 11 - \frac{2}{3} n_f \quad \beta_1 = 102 - \frac{38}{3} n_f,$$

The solution of Eq.(3.2), with the initial condition

$$\alpha(\lambda)|_{\lambda=1} = \alpha \equiv \alpha_s(Q^2)/\pi,$$

is [35]

$$\frac{\alpha(\lambda)}{\alpha} = \left[1 + \alpha \frac{\beta_0}{4} \ln \lambda - \frac{\alpha \beta_1}{4 \beta_0} \left(\frac{\ln \alpha(\lambda)}{\alpha} - \ln \frac{4 \beta_0 / \beta_1 + \alpha(\lambda)}{4 \beta_0 / \beta_1 + \alpha} \right) \right]^{-1}. \quad (3.3)$$

This transcendental equation can be solved iteratively by keeping the leading $\alpha^k \ln^k \lambda$ and next-to-leading $\alpha^k \ln^{k-1} \lambda$ powers. For $\lambda = (1 - x)$ these terms are given by

$$\alpha((1-x)Q^2) = \frac{\alpha_s}{1 + \ln \lambda/t} - \frac{\alpha_s^2 \beta_1 \ln[1 + \ln \lambda/t]}{4\pi \beta_0 [1 + \ln \lambda/t]^2} \quad (3.4)$$

The first term in Eq.(3.4) is the solution of the renormalization group Eq.(3.2) with leading power accuracy, whereas the whole expression (3.4) is the solution of Eq.(3.2) with

next-to-leading power accuracy. After substituting Eq.(3.4) into Eq.(2.10) we get:

$$\begin{aligned}
D(\hat{t}, \hat{u}) &= e_1 \hat{t} \int_0^1 dx \frac{\alpha_s(\lambda \mu_{R_0}^2) \Phi_M(x, p_T^2)}{1-x} + e_2 \hat{u} \int_0^1 dx \frac{\alpha_s(\lambda \mu_{R_0}^2) \Phi_M(x, p_T^2)}{1-x} = \\
&e_1 \hat{t} \alpha_s(-\hat{u}) \int_0^1 dx_1 \frac{\Phi_M(x, p_T^2)}{(1-x)(1+\ln \lambda/t_1)} - e_1 \hat{t} \frac{\alpha_s^2(-\hat{u}) \beta_1}{4\pi \beta_0} \int_0^1 dx \frac{\Phi_M(x, p_T^2) \ln(1+\ln \lambda/t_1)}{(1-x)(1+\ln \lambda/t_1)^2} + \\
&e_2 \hat{u} \alpha_s(-\hat{t}) \int_0^1 dx_1 \frac{\Phi_M(x, p_T^2)}{(1-x)(1+\ln \lambda/t_2)} - e_2 \hat{u} \frac{\alpha_s^2(-\hat{t}) \beta_1}{4\pi \beta_0} \int_0^1 dx \frac{\Phi_M(x, p_T^2) \ln(1+\ln \lambda/t_2)}{(1-x)(1+\ln \lambda/t_2)^2} = \\
&e_1 \hat{t} \alpha_s(-\hat{u}) \int_0^1 dx \frac{\Phi_{asy}(x) \left[1 + \sum_{2,4,..}^{\infty} a_n(\mu_0^2) \left[\frac{\alpha_s(p_T^2)}{\alpha_s(\mu_0^2)} \right]^{\gamma_n/\beta_0} C_n^{3/2}(2x-1) \right]}{(1-x)(1+\ln \lambda/t_1)} - \\
&e_1 \hat{t} \frac{\alpha_s^2(-\hat{u}) \beta_1}{4\pi \beta_0} \int_0^1 dx \frac{\Phi_{asy}(x) \left[1 + \sum_{2,4,..}^{\infty} a_n(\mu_0^2) \left[\frac{\alpha_s(p_T^2)}{\alpha_s(\mu_0^2)} \right]^{\gamma_n/\beta_0} C_n^{3/2}(2x-1) \right] \ln(1+\ln \lambda/t_1)}{(1-x)(1+\ln \lambda/t_1)^2} + \\
&e_2 \hat{u} \alpha_s(-\hat{t}) \int_0^1 dx \frac{\Phi_{asy}(x) \left[1 + \sum_{2,4,..}^{\infty} a_n(\mu_0^2) \left[\frac{\alpha_s(Q^2)}{\alpha_s(\mu_0^2)} \right]^{\gamma_n/\beta_0} C_n^{3/2}(2x-1) \right]}{(1-x)(1+\ln \lambda/t_2)} - \\
&e_2 \hat{u} \frac{\alpha_s^2(-\hat{t}) \beta_1}{4\pi \beta_0} \int_0^1 dx \frac{\Phi_{asy}(x) \left[1 + \sum_{2,4,..}^{\infty} a_n(\mu_0^2) \left[\frac{\alpha_s(p_T^2)}{\alpha_s(\mu_0^2)} \right]^{\gamma_n/\beta_0} C_n^{3/2}(2x-1) \right] \ln(1+\ln \lambda/t_2)}{(1-x)(1+\ln \lambda/t_2)^2}
\end{aligned} \tag{3.5}$$

where $t_1 = 4\pi/\alpha_s(-\hat{u})\beta_0$ and $t_2 = 4\pi/\alpha_s(-\hat{t})\beta_0$.

It should be note that in [41], we used $t_1 \simeq t_2$.

The integral (3.5) is common and, of course, still divergent, but now it is recast into a form, which is suitable for calculation. Using the running coupling constant approach, this integral may be found as a perturbative series in $\alpha_s(Q^2)$

$$D(\hat{t}, \hat{u}) \sim \sum_{n=1}^{\infty} \left(\frac{\alpha_s}{4\pi} \right)^n S_n. \tag{3.6}$$

The expression coefficients S_n can be written as power series in the number of light quark flavors or, equivalently, as a series in power of β_0 :

$$S_n = C_n \beta_0^{n-1}$$

The coefficients C_n of this series demonstrate factorial growth $C_n \sim (n-1)!$, which might indicate an infrared renormalon nature of divergences in the integral (3.5) and corresponding

series (3.6). The procedure for dealing with such ill-defined series is well known: one has to perform the Borel transform of the series [15]

$$B[D](u) = \sum_{n=0}^{\infty} \frac{D_n}{n!} u^n,$$

then invert $B[D](u)$ to obtain the resummed expression (the Borel sum) $D(\hat{t}, \hat{u})$. After this we can find directly the resummed expression for $D(Q^2)$. The change of the variable x to $z = \ln(1 - x)$, as $\ln(1 - x) = \ln \lambda$. Then

$$\begin{aligned} D(\hat{t}, \hat{u}) = & e_1 \hat{t} \alpha_s(-\hat{u}) t_1 \int_0^1 dx \frac{\Phi_M(x, p_T^2)}{(1-x)(t_1+z)} - e_1 \hat{t} \frac{\alpha_s^2(-\hat{u}) \beta_1 t_1^2}{4\pi\beta_0} \int_0^1 dx \frac{\Phi_M(x, p_T^2) \ln(1+z/t_1)}{(1-x)(t_1+z)^2} + \\ & e_2 \hat{u} \alpha_s(-\hat{t}) t_2 \int_0^1 dx \frac{\Phi_M(x, p_T^2)}{(1-x)(t_2+z)} - e_2 \hat{u} \frac{\alpha_s^2(-\hat{t}) \beta_1 t_2^2}{4\pi\beta_0} \int_0^1 dx \frac{\Phi_M(x, p_T^2) \ln(1+z/t_2)}{(1-x)(t_2+z)^2} \end{aligned} \quad (3.7)$$

The basic theoretical problem is how to define the Borel sum $B[D](u)$ of the integral in Eq.(3.7) for the quantities we are interested in. In QCD this problem is usually solved using perturbative methods and calculating the corresponding multiloop Feynman diagrams with a one-gluon line, dressed by the chains of fermion bubbles.

For the calculation the expression (3.7) we will apply the integral representations of $1/(t+z)^\nu$ and $\ln(t+z)/(t+z)^2$ [54,55]. After this operation, formula (3.7) is simplified and we can extract the Borel sum of the perturbative series (3.6) and the corresponding Borel transform in dependence from the wave functions of the meson, respectively. Also after such manipulations the obtained expression can be used for numerical computations.

It is convenient to use the following integral representation for $1/(t+z)^\nu$ and $\ln(t+z)/(t+z)^2$:

$$\frac{1}{(t+z)^\nu} = \frac{1}{\Gamma(\nu)} \int_0^\infty e^{-(t+z)u} u^{\nu-1} du, \text{Re}\nu > 0 \quad (3.8)$$

and

$$\frac{\ln(t+z)}{(t+z)^2} = \int_0^\infty e^{-(t+z)u} (1-C-\ln u) u du \quad (3.9)$$

where $C \simeq 0.577216$ is the Euler-Mascheroni constant.

After inserting Eq.(3.8) and (3.9) into (3.7). then, we obtain

$$\begin{aligned} D(\hat{t}, \hat{u}) = & e_1 \hat{t} \alpha_s(-\hat{u}) t_1 \int_0^1 \int_0^\infty \frac{\Phi_M(x, p_T^2) e^{-(t_1+z)u} du dx}{(1-x)} - \\ & \frac{e_1 \hat{t} \alpha_s^2(-\hat{u}) \beta_1 t_1^2}{4\pi\beta_0} \int_0^1 \int_0^\infty \frac{\Phi_M(x, p_T^2) e^{-(t_1+z)u} du dx}{(1-x)} + \end{aligned}$$

$$\begin{aligned}
& e_2 \hat{u} \alpha_s(-\hat{t}) t_2 \int_0^1 \int_0^\infty \frac{\Phi_M(x, p_T^2) e^{-(t_2+z)u} du dx}{(1-x)} - \\
& \frac{e_2 \hat{u} \alpha_s^2(-\hat{t}) \beta_1 t_2^2}{4\pi \beta_0} \int_0^1 \int_0^\infty \frac{\Phi_M(x, p_T^2) e^{-(t_2+z)u} du dx}{(1-x)}. \tag{3.10}
\end{aligned}$$

In the case of $\Phi_{asy}(x)$ for $D(\hat{t}, \hat{u})$, we get

$$\begin{aligned}
D(\hat{t}, \hat{u}) &= \frac{4\sqrt{3}\pi f_\pi e_1 \hat{t}}{\beta_0} \cdot \int_0^\infty du e^{-t_1 u} \left[\frac{1}{1-u} - \frac{1}{2-u} \right] - \frac{4\sqrt{3}\pi f_\pi e_1 \beta_1 \hat{t}}{\beta_0^3} \\
& \int_0^\infty du e^{-t_1 u} \left[\frac{1}{1-u} - \frac{1}{2-u} \right] (1-C - \ln u - \ln t_1) u + \\
& \frac{4\sqrt{3}\pi f_\pi e_2 \hat{u}}{\beta_0} \cdot \int_0^\infty du e^{-t_2 u} \left[\frac{1}{1-u} - \frac{1}{2-u} \right] - \frac{4\sqrt{3}\pi f_\pi e_2 \beta_1 \hat{u}}{\beta_0^3} \\
& \int_0^\infty du e^{-t_2 u} \left[\frac{1}{1-u} - \frac{1}{2-u} \right] (1-C - \ln u - \ln t_2) u. \tag{3.11}
\end{aligned}$$

In the case of the $\Phi_{CZ}(x, Q^2)$ wave function, we find

$$\begin{aligned}
D(\hat{t}, \hat{u}) &= \frac{4\sqrt{3}\pi f_\pi e_1 \hat{t}}{\beta_0} \cdot \int_0^\infty du e^{-t_1 u} \left[\frac{1}{1-u} - \frac{1}{2-u} + \right. \\
& 0.84 \left[\frac{\alpha_s(p_T^2)}{\alpha_s(\mu_0^2)} \right]^{50/81} \left[\frac{4}{1-u} - \frac{24}{2-u} + \frac{40}{3-u} - \frac{20}{4-u} \right] \left. - \right. \\
& \frac{4\sqrt{3}\pi f_\pi e_1 \beta_1 \hat{t}}{\beta_0^3} \cdot \int_0^\infty du e^{-t_1 u} \left[\frac{1}{1-u} - \frac{1}{2-u} + \right. \\
& 0.84 \left[\frac{\alpha_s(p_T^2)}{\alpha_s(\mu_0^2)} \right]^{50/81} \left[\frac{4}{1-u} - \frac{24}{2-u} + \frac{40}{3-u} - \frac{20}{4-u} \right] \left. (1-C - \ln u - \ln t_1) u + \right. \\
& \frac{4\sqrt{3}\pi f_\pi e_2 \hat{u}}{\beta_0} \cdot \int_0^\infty du e^{-t_2 u} \left[\frac{1}{1-u} - \frac{1}{2-u} + \right. \\
& 0.84 \left[\frac{\alpha_s(p_T^2)}{\alpha_s(\mu_0^2)} \right]^{50/81} \left[\frac{4}{1-u} - \frac{24}{2-u} + \frac{40}{3-u} - \frac{20}{4-u} \right] \left. - \right. \\
& \frac{4\sqrt{3}\pi f_\pi e_2 \beta_1 \hat{u}}{\beta_0^3} \int_0^\infty du e^{-t_2 u} \left[\frac{1}{1-u} - \frac{1}{2-u} + \right. \\
& 0.84 \left[\frac{\alpha_s(p_T^2)}{\alpha_s(\mu_0^2)} \right]^{50/81} \left[\frac{4}{1-u} - \frac{24}{2-u} + \frac{40}{3-u} - \frac{20}{4-u} \right] \left. (1-C - \ln u - \ln t_2) u \right. \tag{3.12}
\end{aligned}$$

In the case of the $\Phi_{CLEO}(x, Q^2)$ wave function, we get

$$D(\hat{t}, \hat{u}) = \frac{4\sqrt{3}\pi f_\pi e_1 \hat{t}}{\beta_0} \int_0^\infty du e^{-t_1 u} \left[\frac{1}{1-u} - \frac{1}{2-u} + 0.405 \left[\frac{\alpha_s(p_T^2)}{\alpha_s(\mu_0^2)} \right]^{50/81} \right].$$

$$\begin{aligned}
& \left[\frac{4}{1-u} - \frac{24}{2-u} + \frac{40}{3-u} - \frac{20}{4-u} \right] - 0.4125 \left[\frac{\alpha_s(p_T^2)}{\alpha_s(\mu_0^2)} \right]^{364/405} \\
& \left[\frac{8}{1-u} - \frac{120}{2-u} + \frac{560}{3-u} - \frac{1112}{4-u} + \frac{1008}{5-u} - \frac{336}{6-u} \right] - \\
& \frac{4\sqrt{3}\pi f_\pi e_1 \beta_1 \hat{t}}{\beta_0^3} \int_0^\infty du e^{-t_1 u} \left[\frac{1}{1-u} - \frac{1}{2-u} + 0.405 \left[\frac{\alpha_s(p_T^2)}{\alpha_s(\mu_0^2)} \right]^{50/81} \right. \\
& \left. \left[\frac{4}{1-u} - \frac{24}{2-u} + \frac{40}{3-u} - \frac{20}{4-u} \right] - 0.4125 \left[\frac{\alpha_s(Q^2)}{\alpha_s(\mu_0^2)} \right]^{364/405} \right. \\
& \left. \left[\frac{8}{1-u} - \frac{120}{2-u} + \frac{560}{3-u} - \frac{1112}{4-u} + \frac{1008}{5-u} - \frac{336}{6-u} \right] \right] (1 - C - \ln u - \ln t_1) u + \\
& \frac{4\sqrt{3}\pi f_\pi e_2 \hat{u}}{\beta_0} \int_0^\infty du e^{-t_2 u} \left[\frac{1}{1-u} - \frac{1}{2-u} + 0.405 \left[\frac{\alpha_s(p_T^2)}{\alpha_s(\mu_0^2)} \right]^{50/81} \right. \\
& \left. \left[\frac{4}{1-u} - \frac{24}{2-u} + \frac{40}{3-u} - \frac{20}{4-u} \right] - 0.4125 \left[\frac{\alpha_s(p_T^2)}{\alpha_s(\mu_0^2)} \right]^{364/405} \right. \\
& \left. \left[\frac{8}{1-u} - \frac{120}{2-u} + \frac{560}{3-u} - \frac{1112}{4-u} + \frac{1008}{5-u} - \frac{336}{6-u} \right] \right] - \\
& \frac{4\sqrt{3}\pi f_\pi e_2 \beta_1 \hat{u}}{\beta_0^3} \int_0^\infty du e^{-t_2 u} \left[\frac{1}{1-u} - \frac{1}{2-u} + 0.405 \left[\frac{\alpha_s(p_T^2)}{\alpha_s(\mu_0^2)} \right]^{50/81} \right. \\
& \left. \left[\frac{4}{1-u} - \frac{24}{2-u} + \frac{40}{3-u} - \frac{20}{4-u} \right] - 0.4125 \left[\frac{\alpha_s(p_T^2)}{\alpha_s(\mu_0^2)} \right]^{364/405} \right. \\
& \left. \left[\frac{8}{1-u} - \frac{120}{2-u} + \frac{560}{3-u} - \frac{1112}{4-u} + \frac{1008}{5-u} - \frac{336}{6-u} \right] \right] (1 - C - \ln u - \ln t_2) u \quad (3.13)
\end{aligned}$$

Also, in the case of the $\Phi_{BMS}(x, Q^2)$ wave function, we get

$$\begin{aligned}
D(\hat{t}, \hat{u}) &= \frac{4\sqrt{3}\pi f_\pi e_1 \hat{t}}{\beta_0} \int_0^\infty du e^{-t_1 u} \left[\frac{1}{1-u} - \frac{1}{2-u} + 0.282 \left[\frac{\alpha_s(p_T^2)}{\alpha_s(\mu_0^2)} \right]^{50/81} \right. \\
& \left. \left[\frac{4}{1-u} - \frac{24}{2-u} + \frac{40}{3-u} - \frac{20}{4-u} \right] - 0.244 \left[\frac{\alpha_s(p_T^2)}{\alpha_s(\mu_0^2)} \right]^{364/405} \right. \\
& \left. \left[\frac{8}{1-u} - \frac{120}{2-u} + \frac{560}{3-u} - \frac{1112}{4-u} + \frac{1008}{5-u} - \frac{336}{6-u} \right] \right] - \\
& \frac{4\sqrt{3}\pi f_\pi e_1 \beta_1 \hat{t}}{\beta_0^3} \int_0^\infty du e^{-t_1 u} \left[\frac{1}{1-u} - \frac{1}{2-u} + 0.282 \left[\frac{\alpha_s(p_T^2)}{\alpha_s(\mu_0^2)} \right]^{50/81} \right. \\
& \left. \left[\frac{4}{1-u} - \frac{24}{2-u} + \frac{40}{3-u} - \frac{20}{4-u} \right] - 0.244 \left[\frac{\alpha_s(p_T^2)}{\alpha_s(\mu_0^2)} \right]^{364/405} \right. \\
& \left. \left[\frac{8}{1-u} - \frac{120}{2-u} + \frac{560}{3-u} - \frac{1112}{4-u} + \frac{1008}{5-u} - \frac{336}{6-u} \right] \right] (1 - C - \ln u - \ln t_1) u +
\end{aligned}$$

$$\begin{aligned}
& \frac{4\sqrt{3}\pi f_\pi e_2 \hat{u}}{\beta_0} \int_0^\infty du e^{-t_2 u} \left[\frac{1}{1-u} - \frac{1}{2-u} + 0.282 \left[\frac{\alpha_s(p_T^2)}{\alpha_s(\mu_0^2)} \right]^{50/81} \right. \\
& \quad \left[\frac{4}{1-u} - \frac{24}{2-u} + \frac{40}{3-u} - \frac{20}{4-u} \right] - 0.244 \left[\frac{\alpha_s(p_T^2)}{\alpha_s(\mu_0^2)} \right]^{364/405} \\
& \quad \left. \left[\frac{8}{1-u} - \frac{120}{2-u} + \frac{560}{3-u} - \frac{1112}{4-u} + \frac{1008}{5-u} - \frac{336}{6-u} \right] \right] - \\
& \frac{4\sqrt{3}\pi f_\pi e_2 \beta_1 \hat{u}}{\beta_0^3} \int_0^\infty du e^{-t_2 u} \left[\frac{1}{1-u} - \frac{1}{2-u} + 0.282 \left[\frac{\alpha_s(p_T^2)}{\alpha_s(\mu_0^2)} \right]^{50/81} \right. \\
& \quad \left[\frac{4}{1-u} - \frac{24}{2-u} + \frac{40}{3-u} - \frac{20}{4-u} \right] - 0.244 \left[\frac{\alpha_s(p_T^2)}{\alpha_s(\mu_0^2)} \right]^{364/405} \\
& \quad \left. \left[\frac{8}{1-u} - \frac{120}{2-u} + \frac{560}{3-u} - \frac{1112}{4-u} + \frac{1008}{5-u} - \frac{336}{6-u} \right] \right] (1 - C - \ln u - \ln t_2) u \quad (3.14)
\end{aligned}$$

Equations(3.11)-(3.14) is nothing more than the Borel sum of the perturbative series (3.6), and the corresponding Borel transform in the case $\Phi_{asy}(x)$ is

$$B[D](u) = \frac{1}{1-u} - \frac{1}{2-u}, \quad (3.15)$$

in the case $\Phi_{CZ}(x, Q^2)$ is

$$B[D](u) = \frac{1}{1-u} - \frac{1}{2-u} + 0.84 \left(\frac{\alpha_s(p_T^2)}{\alpha_s(\mu_0^2)} \right)^{50/81} \left(\frac{4}{1-u} - \frac{24}{2-u} + \frac{40}{3-u} - \frac{20}{4-u} \right), \quad (3.16)$$

in the case $\Phi_{CLEO}(x, Q^2)$ is

$$\begin{aligned}
B[D](u) &= \frac{1}{1-u} - \frac{1}{2-u} + 0.405 \left(\frac{\alpha_s(p_T^2)}{\alpha_s(\mu_0^2)} \right)^{50/81} \left(\frac{4}{1-u} - \frac{24}{2-u} + \frac{40}{3-u} - \frac{20}{4-u} \right) - \\
& 0.4125 \left(\frac{\alpha_s(Q^2)}{\alpha_s(\mu_0^2)} \right)^{364/405} \left(\frac{8}{1-u} - \frac{120}{2-u} + \frac{560}{3-u} - \frac{1112}{4-u} + \frac{1008}{5-u} - \frac{336}{6-u} \right). \quad (3.17)
\end{aligned}$$

and in the case $\Phi_{BMS}(x, Q^2)$ is

$$\begin{aligned}
B[D](u) &= \frac{1}{1-u} - \frac{1}{2-u} + 0.282 \left(\frac{\alpha_s(p_T^2)}{\alpha_s(\mu_0^2)} \right)^{50/81} \left(\frac{4}{1-u} - \frac{24}{2-u} + \frac{40}{3-u} - \frac{20}{4-u} \right) - \\
& 0.244 \left(\frac{\alpha_s(p_T^2)}{\alpha_s(\mu_0^2)} \right)^{364/405} \left(\frac{8}{1-u} - \frac{120}{2-u} + \frac{560}{3-u} - \frac{1112}{4-u} + \frac{1008}{5-u} - \frac{336}{6-u} \right). \quad (3.18)
\end{aligned}$$

The series (3.6) can be recovered by means of the following formula

$$C_n = \left(\frac{d}{du} \right)^{n-1} B[D](u) |_{u=0}$$

The Borel transform $B[D](u)$ has poles on the real u axis at $u = 1; 2; 3; 4; 5; 6$, which confirms our conclusion concerning the infrared renormalon nature of divergences in (3.6). To remove them from Eqs.(3.11)-(3.14) we applied the principal value prescription.

Hence, the effective cross section obtained after substitution of the expressions (3.10-3.14) into the expression (2.10) is referred as the running coupling effective cross section. We will denote the higher-twist cross section obtained using the running coupling constant approach by $(\Sigma_\pi^{HT})^{res}$.

IV. CONTRIBUTION OF THE LEADING-TWIST DIAGRAMS

Regarding the higher-twist corrections to the pion production cross section, a comparison of our results with leading-twist contributions is crucial. We take two leading-twist subprocesses for the pion production:(1) quark-antiquark annihilation $q\bar{q} \rightarrow g\gamma$, in which the π meson is indirectly emitted from the gluon, $g \rightarrow \pi^+(\pi^-)$ and (2) quark-gluon fusion, $qg \rightarrow q\gamma$, with subsequent fragmentation of the final quark into a meson, $q \rightarrow \pi^+(\pi^-)$. The corresponding cross sections are obtained in

$$\frac{d\sigma}{d\hat{t}}(q\bar{q} \rightarrow gq) = \frac{8}{9}\pi\alpha_E\alpha_s(Q^2)\frac{e_q^2}{\hat{s}^2}\left(\frac{\hat{t}}{\hat{u}} + \frac{\hat{u}}{\hat{t}}\right), \quad (4.1)$$

$$\frac{d\sigma}{d\hat{t}}(qg \rightarrow q\gamma) = -\frac{\pi e_q^2\alpha_E\alpha_s(Q^2)}{3\hat{s}^2}\left(\frac{\hat{s}}{\hat{t}} + \frac{\hat{t}}{\hat{s}}\right). \quad (4.2)$$

For the leading-twist contribution, we find

$$\begin{aligned} \Sigma_M^{LT} \equiv E\frac{d\sigma}{d^3p} = \sum_q \int_0^1 dx_1 dx_2 dz \left(G_{q_1/h_1}(x_1)G_{q_2/h_2}(x_2)D_g^\pi(z)\frac{\hat{s}}{\pi z^2}\frac{d\sigma}{d\hat{t}}(q\bar{q} \rightarrow g\gamma) + \right. \\ \left. G_{q_1/h_1}(x_1)G_{g/h_2}(x_2)D_q^\pi(z)\frac{\hat{s}}{\pi z^2}\frac{d\sigma}{d\hat{t}}(qg \rightarrow q\gamma) \right) \delta(\hat{s} + \hat{t} + \hat{u}), \end{aligned} \quad (4.3)$$

where

$$\hat{s} = x_1 x_2 s, \quad \hat{t} = \frac{x_1 t}{z}, \quad \hat{u} = \frac{x_2 u}{z}, \quad z = -\frac{x_1 t + x_2 u}{x_1 x_2 s}. \quad (4.4)$$

$D_g^\pi(z) = D_g^{\pi^+}(z) = D_g^{\pi^-}(z)$ and $D_q^\pi(z)$ represents gluon and quark fragmentation functions into a meson containing gluon and quark of the same flavor. In the leading-twist subprocess, the π meson is indirectly emitted from the gluon and quark with the fractional momentum z . The δ function can be expressed in terms of the parton kinematic variables, and the z

integration can then be done. The final form for the cross section is

$$\begin{aligned}
\Sigma_M^{LT} \equiv E \frac{d\sigma}{d^3p} = & \sum_q \int_{x_{1min}}^1 dx_1 \int_{x_{2min}}^1 dx_2 \left(G_{q_1/h_1}(x_1) G_{q_2/h_2}(x_2) D_g^\pi(z) \cdot \frac{1}{\pi z} \frac{d\sigma}{d\hat{t}}(q\bar{q} \rightarrow g\gamma) + \right. \\
& \left. G_{q_1/h_1}(x_1) G_{g/h_2}(x_2) D_g^\pi(z) \cdot \frac{1}{\pi z} \frac{d\sigma}{d\hat{t}}(qg \rightarrow q\gamma) \right) = \\
\sum_q \int_{x_{1min}}^1 dx_1 \int_{x_{2min}}^1 & \frac{dx_2}{-(x_1 t + x_2 u)} \left(x_1 G_{q_1/h_1}(x_1) s x_2 G_{q_2/h_2}(x_2) \frac{D_g^\pi(z)}{\pi} \frac{d\sigma}{d\hat{t}}(q\bar{q} \rightarrow g\gamma) + \right. \\
& \left. x_1 G_{q_1/h_1}(x_1) s x_2 G_{g/h_2}(x_2) \frac{D_g^\pi(z)}{\pi} \frac{d\sigma}{d\hat{t}}(qg \rightarrow q\gamma) \right). \tag{4.5}
\end{aligned}$$

V. NUMERICAL RESULTS AND DISCUSSION

In this section, we discuss the numerical results for next-to-leading order higher-twist effects with higher-twist contributions calculated in the context of the running coupling and frozen coupling approaches on the dependence of the chosen meson wave functions in the process $pp \rightarrow \pi^+(or \pi^-)\gamma + X$. In the calculations, we use the asymptotic wave function Φ_{asy} , the Chernyak-Zhitnitsky Φ_{CZ} , the CLEO pion wave function [41], the Braun-Filyanov pion wave functions [42], and the Bakulev-Mikhailov-Stefanis pion wave function[43]. For the higher-twist subprocess, we take $q_1 + \bar{q}_2 \rightarrow (q_1 \bar{q}_2) + \gamma$ and we have extracted the following four higher-twist subprocesses contributing to $pp \rightarrow \pi^+(or \pi^-)\gamma$ cross sections: $u\bar{d} \rightarrow \pi^+\gamma$, $\bar{d}u \rightarrow \pi^+\gamma$, $\bar{u}d \rightarrow \pi^-\gamma$, $d\bar{u} \rightarrow \pi^-\gamma$ contributing to cross sections. For the dominant leading-twist subprocess for the pion production, we take the quark-antiquark annihilation $q\bar{q} \rightarrow g\gamma$, in which the π meson is indirectly emitted from the gluon and quark-gluon fusion, $qg \rightarrow q\gamma$, with subsequent fragmentation of the final quark into a meson, $q \rightarrow \pi^+(\pi^-)$. As an example for the quark distribution function inside the proton, the MRST2003c package [56] has been used. The higher twist subprocesses probe the meson wave functions over a large range of Q^2 squared momentum transfer, carried by the gluon. Therefore, in the diagram given in Fig.1 we take $Q_1^2 = (x_1 - 1)\hat{u}$, $Q_2^2 = -x_1\hat{t}$, which we have obtained directly from the higher-twist subprocesses diagrams. The same Q^2 has been used as an argument of $\alpha_s(Q^2)$ in the calculation of each diagram.

The results of our numerical calculations are plotted in Figs.2-15. First of all, it is very interesting to compare the resummed higher-twist cross sections with the ones obtained in the

framework of the frozen coupling approach. In Figs.2-4 we show the dependence of next-to-leading order higher-twist cross sections $(\Sigma_{\pi^+}^{HT})_{NLO}^{res}$ calculated in the context of the running coupling constant approach and the ratios $R = (\Sigma_{\pi^+}^{HT})_{NLO}^{res}/(\Sigma_{\pi^+}^{HT})_{LO}^0$, $(\Sigma_{\pi^+}^{HT})_{NLO}^{res}/(\Sigma_{\pi^+}^{HT})_{LO}^{res}$ as a function of the pion transverse momentum p_T for different pion wave functions at $y = 0$. It is seen that the values of cross sections $(\Sigma_{\pi^+}^{HT})_{NLO}^{res}$, and ratios for fixed y and \sqrt{s} depend on the choice of the pion wave function. As seen from Fig.2 the next-to-leading order higher-twist differential cross section is monotonically decreasing with an increase in the transverse momentum of the pion. In Figs.3-5, we show the dependence of the ratios $R = (\Sigma_{\pi^+}^{HT})_{NLO}^{res}/(\Sigma_{\pi^+}^{HT})_{LO}^0$, $(\Sigma_{\pi^+}^{HT})_{NLO}^{res}/(\Sigma_{\pi^+}^{HT})_{LO}^{res}$, $(\Sigma_{\pi^+}^{HT})_{NLO}^{res}/(\Sigma_{\pi^+}^{LT})$ as a function of the pion transverse momentum p_T for different pion wave functions. Here $(\Sigma_{\pi^+}^{HT})_{NLO}^{res}$, $(\Sigma_{\pi^+}^{HT})_{LO}^0$, $(\Sigma_{\pi^+}^{LT})$ are the higher-twist cross sections calculated in the context of the running coupling method, in the framework of the frozen coupling approach and is the leading-twist cross section, respectively. As seen from Fig.5, in the region $2 \text{ GeV}/c < p_T < 4 \text{ GeV}/c$ next-to-leading order higher-twist cross section calculated in the context of the running coupling method is suppressed by about 1-2 orders of magnitude relative to the leading-twist cross section, but in the region $5 \text{ GeV}/c < p_T \leq 30 \text{ GeV}/c$ is comparable with the cross section of leading-twist. In Figs.6-8, we have depicted next-to-leading order higher-twist cross sections $(\Sigma_{\pi^+}^{HT})_{NLO}^{res}$, ratios $R = (\Sigma_{\pi^+}^{HT})_{NLO}^{res}/(\Sigma_{\pi^+}^{HT})_{LO}^{res}$, $(\Sigma_{\pi^+}^{HT})_{NLO}^{res}/(\Sigma_{\pi^+}^{LT})$ as a function of the rapidity y of the pion at $\sqrt{s} = 62.4 \text{ GeV}$ and $p_T = 4.9 \text{ GeV}/c$. At $\sqrt{s} = 62.4 \text{ GeV}$ and $p_T = 4.9 \text{ GeV}/c$, the pion rapidity lies in the region $-2.52 \leq y \leq 2.52$.

As seen from Figs.6-8, next-to-leading order higher-twist cross section and ratios have a different distinctive. In the region $(0.2 \leq y \leq 2.52)$ the next-to-leading order higher-twist cross section $(\Sigma_{\pi^+}^{HT})_{NLO}^{res}$, is suppressed by about 1-2 order of magnitude relative to the leading-twist cross section. In the region $(-2.52 \leq y \leq -1.92)$, the ratio for all wave functions increase with an increase of the y rapidity of the pion and has a maximum approximately at the point $y = -1.92$. Besides that, the ratio decreases with an increase in the y rapidity of the pion. As is seen from Figs.7-8, the ratio R very sensitive to the choice of the meson wave functions. But, as seen from Fig.8, the ratio $(\Sigma_{\pi^+}^{HT})_{NLO}^{res}/(\Sigma_{\pi^+}^{LT})$ for all wave functions has a minimum approximately at the point $y = -1.92$. Also, the distinction between $R(\Phi_{asy}(x))$ with $R(\Phi_{CLEO}(x, Q^2))$, $R(\Phi_{CZ}(x, Q^2))$, $R(\Phi_{BF}(x, Q^2))$ and $R(\Phi_{BMS}(x, Q^2))$ have been calculated. For example, in the case of $\sqrt{s} = 62.4 \text{ GeV}$, $y = 0$, the distinction between $R(\Phi_{asy}(x))$ with $R(\Phi_i(x, Q^2))$ ($i=CLEO$,

CZ, BF, BMS) as a function of the pion transverse momentum p_T is shown in Table I. Thus, the distinction between $R(\Phi_{asy}(x))$ and $R(\Phi_i(x, Q^2))(i = CLEO, CZ, BF)$ is maximum at $p_T = 20 \text{ GeV}/c$, with $R(\Phi_{BMS}(x))$ at $p_T = 2 \text{ GeV}/c$ but the distinction between $R(\Phi_{asy}(x))$ with $R(\Phi_i(x, Q^2))(i = CLEO, CZ, BF)$ is minimum at $p_T = 2 \text{ GeV}/c$, with $R(\Phi_{BMS}(x))$ at $p_T = 20 \text{ GeV}/c$ and increase with an increase in p_T . Such a behavior of R may be explained by reducing all moments of the pion model wave functions to those of $\Phi_{asy}(x)$ for high Q^2 . Also, we have calculated the distinction between $R(\Phi_{asy}(x))$ with $R(\Phi_{CLEO}(x, Q^2))$, $R(\Phi_{CZ}(x, Q^2))$, $R(\Phi_{BF}(x, Q^2))$ and $R(\Phi_{BMS}(x, Q^2))$ as a function of the rapidity y of the pion. For example, in the case of $\sqrt{s} = 62.4 \text{ GeV}$, $p_T = 4.9 \text{ GeV}/c$ the distinction between $R(\Phi_{asy}(x))$ with $R(\Phi_i(x, Q^2))$ ($i=CLEO, CZ, BF, BMS$) as a function of the rapidity y of the pion is presented in Table II.

We have also carried out comparative calculations in the center-of-mass energy $\sqrt{s} = 200 \text{ GeV}$. The results of our numerical calculations in the center-of-mass energies $\sqrt{s} = 200 \text{ GeV}$ are plotted in Figs.9-15. Analysis of our calculations at the center-of-mass energies $\sqrt{s} = 62.4 \text{ GeV}$ and $\sqrt{s} = 200 \text{ GeV}$, show that with the increase in beam energy values of the cross sections, ratio $R = (\Sigma_{\pi^+}^{HT})_{NLO}^{res}/(\Sigma_{\pi^+}^{HT})_{LO}^0$, and contributions of next-to-leading order higher-twist to the cross section decrease by about 1-2 order. Therefore the experimental investigation of higher-twist effects include renormalon effects conveniently in low energy. On the other hand, the higher-twist corrections and ratios R a very sensitive to the choice of the pion wave function. Analysis of our calculations at the center-of-mass energies $\sqrt{s} = 62.4 \text{ GeV}$ and $\sqrt{s} = 200 \text{ GeV}$, show that values of the next-to-leading order cross sections decrease by about (25 – 30) percent of magnitude relative to the leading-order cross sections. Also, the distinction between $R(\Phi_{asy}(x))$ with $R(\Phi_{CLEO}(x, Q^2))$, $R(\Phi_{CZ}(x, Q^2))$, $R(\Phi_{BF}(x, Q^2))$ and $R(\Phi_{BMS}(x, Q^2))$ have been calculated. For example, in the case of $\sqrt{s} = 200 \text{ GeV}$, $y = 0$, the distinction between $R(\Phi_{asy}(x))$ with $R(\Phi_i(x, Q^2))$ ($i=CLEO, CZ, BF, BMS$) as a function of the pion transverse momentum p_T is shown in Table III. Thus, the distinction between $R(\Phi_{asy}(x))$ with $R(\Phi_i(x, Q^2))$, ($i= CLEO, BF,$) is maximum at $p_T = 35 \text{ GeV}/c$, with $R(\Phi_{BMS}(x))$ at $p_T = 10 \text{ GeV}/c$, but the distinction between $R(\Phi_{asy}(x))$ with $R(\Phi_{CZ}(x, Q^2))$, $R(\Phi_{CLEO}(x, Q^2))$, $R(\Phi_{BF}(x, Q^2))$ is minimum at $p_T = 10 \text{ GeV}/c$, with $R(\Phi_{BMS}(x))$ at $p_T = 95 \text{ GeV}/c$ and increase with an increase in p_T . Also, we have calculated the distinction between $R(\Phi_{asy}(x))$ with $R(\Phi_{CLEO}(x, Q^2))$, $R(\Phi_{CZ}(x, Q^2))$, $R(\Phi_{BF}(x, Q^2))$ and $R(\Phi_{BMS}(x, Q^2))$ as a function of the rapidity y of the

pion. For example, in the case of $\sqrt{s} = 200\text{GeV}$, $p_T = 15.5\text{GeV}/c$ the distinction between $R(\Phi_{asy}(x))$ with $R(\Phi_i(x, Q^2))$ as a function of the rapidity y of the pion is presented in Table IV. The calculations show that the ratio $R(\Phi_i(x, Q^2))/R(\Phi_{asy}(x))$, ($i=\text{CLEO, CZ, BF, BMS}$) for all values of the transverse momentum p_T of the pion identically equivalent to ratio $r(\Phi_i(x, Q^2))/r(\Phi_{asy}(x))$.

In our calculations of the next-to-leading order higher-twist cross section of the process the dependence of the transverse momentum of meson appears in the range of $(10^{-5} \div 10^{-25})\text{mb}/\text{GeV}^2$. Therefore, higher-twist cross section obtained in our paper should be observable at RHIC

VI. CONCLUDING REMARKS

In this work we have calculated the inclusive meson production via higher-twist mechanism and obtained the expressions for the subprocess $q\bar{q} \rightarrow M\gamma$ cross section for mesons with symmetric wave functions. For calculation of the next-to-leading order cross section we have applied the running coupling constant method and revealed infrared renormalon poles in the cross section expression. Infrared renormalon induced divergences have been regularized by the means of the principal value prescription and the resummed expression (the Borel sum) for the next-to-leading order higher-twist cross section has been found. In the resummed higher-twist cross section differs considerably from that found using the frozen coupling approach, some regions. Also we have demonstrated that next-to-leading order higher-twist contributions to meson production cross section in the proton-proton collisions have important phenomenological consequences. Our investigation enables us to conclude that the higher-twist pion production cross section in the proton-proton collisions depends on the form of the pion model wave functions and may be used for their study. Analysis of our calculations shows that the magnitude of next-to-leading order cross sections calculated in the running coupling approach in some regions is larger than the leading-twist cross sections in 1-2 order.

Further investigations are needed in order to clarify the role of high twist effects in this process. We have demonstrated that the resummed result depends on the pion model wave functions used in calculations. The proton-proton collisions provide us with a new opportunity to probe a proton's internal structure. In particular, meson production in

proton-proton collisions takes into account infrared renormalon effects: this opens a window toward new types of parton distributions which can not be measured by the deep inelastic lepton-proton scatterings. Finally, we discuss the phenomenological consequences of possible higher-twist contributions to meson production in proton-proton collisions in next-to-leading order at RHIC. Future RHIC measurements will provide further tests of the dynamics of large p_T hadron production beyond leading twist.

Acknowledgments

The work presented in this paper was completed while one of the authors, A.I.Ahmadov, was visiting the HECAP section of the Abdus Salam ICTP, Trieste, Italy. He would like to express his gratitude to the members of the section especially to the head Prof. S. Randjbar-Daemi for their hospitality. Financial support by ICTP is also gratefully acknowledged.

VII. REFERENCES

- [1] G.'t. Hooft, in *The Whys of Subnuclear Physics*, Erice, 1977, edited by A. Zichichi (Plenum, New York, 1979), p.94
- [2] A. H. Mueller, *Nucl. Phys.* **B250**, 327 (1985); *Phys. Lett.* **B308**, 355 (1993).
- [3] V. I. Zakharov, *Nucl. Phys.* **B385**, 452 (1992).
- [4] M. Beneke, *Phys. Rep.* **317**, 1 (1999).
- [5] G. Grunberg, *Phys. Lett.* **B95**, 70 (1980); **B110**, 501(E), (1982); *Phys. Rev.* **D29**, 2315 (1984).
- [6] P. M. Stevenson, *Phys. Rev.* **D23**, 2916 (1981).
- [7] S. J. Brodsky, G. P. Lepage and P. B. Mackenzie, *Phys. Rev.* **D28**, 228 (1983); G. P. Lepage and P. B. Mackenzie, *ibid.* **48**, 2250 (1993).
- [8] G. Grunberg and A. L. Kataev, *Phys. Lett* **B279**, 352 (1992).
- [9] S. J. Brodsky and J. Rathsman, hep-ph/9906339.
- [10] H. J. Lu, and C. A. R. Sa de Melo, *Phys. Lett* **B273**, 260 (1991); **B285**, 399(E) (1992); H. J. Lu, *Phys. Rev.* **D45**, 1217 (1992).
- [11] C. P. Lepage and P. B. Mackenzie *Phys. Rev.* **D48**, 2250 (1993).

- [12] S. J. Brodsky and H. J. Lu, Phys. Rev. **D51**, 3652 (1995).
- [13] J. Rathsman, Phys. Rev. **D54**, 3420 (1996).
- [14] M. Neubert, Phys. Rev. **D51**, 5924 (1995).
- [15] M. Beneke and V. M. Braun, Phys. Lett. **B348**, 513 (1995); P. Ball, M. Beneke and V. M. Braun, Nucl. Phys. **B452**, 424 (1995); M. Beneke, Nucl. Phys. **B405**, 563 (1993).
- [16] C. N. Lovett-Turner and C. J. Maxwell, Nucl. Phys. **B432**, 147 (1994).
- [17] S. J. Brodsky, J. Ellis, E. Gardi, M. Karliner, and M. A. Samuel, Phys. Rev. **D56**, 6980 (1997).
- [18] S. J. Brodsky, G. T. Gabadadze, A. L. Kataev, and H. J. Lu, Phys. Lett. **B372**, 133 (1996).
- [19] S. J. Brodsky, M. Melles, and J. Rathsman, Phys. Rev. **D60**, 096006 (1999).
- [20] S. J. Brodsky, M. S. Gill, M. Melles, and J. Rathsman, Phys. Rev. **D58**, 116006 (1998).
- [21] S. V. Mikhailov, JHEP 0706:009 (2007).
- [22] V. A. Matveev, R. M. Muradyan, and A. N. Tavkhelidze, Lett. Nuovo Cimento 7, 719 (1973).
- [23] S. J. Brodsky and G. R. Farrar, Phys. Rev. Lett. **31**, 1153 (1973).
- [24] J. F. Gunion, S. J. Brodsky, R. Blankenbecler, Phys.Rev. **D6**, 2652 (1972)
- [25] D. W. Sivers, S. J. Brodsky, R. Blankenbecler, Phys. Rept. **23**, 1 (1976).
- [26] V. A. Matveev, L. A. Slepchenko, and A. N. Tavkhelidze, Phys. Lett. **B100**, 75 (1981).
- [27] G. L. Lepage and S. J. Brodsky, Phys. Rev. **D22**, 2157 (1980).
- [28] V. L. Chernyak and A. R. Zhitnitsky, Phys. Rep. **112**, 173 (1984).
- [29] François Arleo and David d’Enterria, Phys. Rev. **D78**: 094004 (2008).
- [30] J. A. Bagger and J. F. Gunion, Phys. Rev. **D25**, 2287 (1982).
- [31] V. N. Baier and A. Grozin, Phys. Lett. **B96**, 181 (1980); S. Gupta, Phys. Rev. **D24**, 1169 (1981).
- [32] A. I. Ahmadov, I. Boztosun, R. Kh. Muradov, A. Soylu and E. A. Dadashov, Int. J. Mod. Phys. **E15**, 1209 (2006).
- [33] M. Maul, E. Stein, A. Schäfer, L. Mankiewich, Phys. Lett.**B401**,100 (1997).
- [34] Y. L. Dokshitzer, V. A. Khoze and S. I. Troyan, Phys. Rev. **D53**, 89 (1996).
- [35] A. L. Kataev, Mod. Phys. Lett. **A20**, 2007 (2005).
- [36] H. Contopanagos and G. Sterman, Nucl. Phys. **B419**, 77 (1994).
- [37] W. Greiner, S. Schramm and E. Stein, Quantum Chromodynamics, 2nd edn.(Berlin, Springer, 2002), pp.551.

- [38] D. V. Shirkov and I. L. Solovtsov, Phys. Rev. Lett. **79**, 1209 (1997).
- [39] STAR Collaboration (J.Adams et.al), Phys. Lett. **B637**, 161 (2006).
- [40] S.S. Agaev, Phys. Lett. **B360**, 117 (1995); **B369**, 379(E) (1996).
- [41] A. I. Ahmadov, Coskun Aydin, Sh. M. Nagiyev, Yilmaz A. Hakan, and E. A. Dadashov, Phys. Rev. **D80**, 016003 (2009).
- [42] A. I. Ahmadov, Coskun Aydin, E. A. Dadashov and Sh. M. Nagiyev, Phys. Rev. **D81**, 054016 (2010).
- [43] S.S. Agaev, Modern Physics Letters **A13**, 2637 (1998).
- [44] François Arleo, Stanley J. Brodsky, Dae Suang Hwang, and Anne M.Sickles, Phys. Rev. Lett. **105**, 062002 (2010).
- [45] S. M. Berman, J. D. Bjorken and J. B. Kogut, Phys. Rev. **D18**, 900 (1978).
- [46] V. L. Chernyak and A. R. Zhitnitsky, Nucl. Phys. **B201**, 492 (1982); V. L. Chernyak, A. R. Zhitnitsky and I. R. Zhitnitsky, Nucl. Phys. **B204**, 477 (1982).
- [47] A. Schmedding and O. Yakovlev, Phys. Rev. **D62**, 116002 (2000).
- [48] V. M. Braun and I. F. Filyanov, Z. Phys, **C44**, 157 (1989).
- [49] A. P. Bakulev, S. V. Mikhailov and N. G. Stefanis, Phys. Lett, **B587**, 91 (2004).
- [50] S. V. Mikhailov and A. V. Radyushkin, Phys. Rev. **D45**, 1754 (1992).
- [51] A. P. Bakulev, S. V. Mikhailov, Z. Phys. **C68**, 451 (1995).
- [52] A. E. Dorokhov, JETP Lett. **77**, 63 (2003).
- [53] J. F. Owens, Rev. Mod. Phys. **59**, 465 (1987).
- [54] J. Zinn-Justin, Phys. Rept. **70**, 109 (1981).
- [55] A. Erdelyi, Higher Transcendental Functions (McGrow-Hill Book Company, New York, 1953), Vol.2.
- [56] MRST2003c.f can be obtained from <http://durpdg.dur.ac.uk/hepdata/pdf.html>. See also, A. D. Martin, R. G. Roberts, W. J. Stirling and R. S.Thorne, hep-ph/0307262; R. S.Thorne, hep-ph/0309343.

$p_T, GeV/c$	$\frac{R(\Phi_{CLEO}(x, Q^2))}{R(\Phi_{asy}(x))}$	$\frac{R(\Phi_{CZ}(x, Q^2))}{R(\Phi_{asy}(x))}$	$\frac{R(\Phi_{BF}(x, Q^2))}{R(\Phi_{asy}(x))}$	$\frac{R(\Phi_{BMS}(x, Q^2))}{R(\Phi_{asy}(x))}$
2	0.391	0.212	0.338	7.628
6	1.236	0.387	1.03	1.632
20	5.169	4.226	4.326	2.268

TABLE I: The distinction between $R(\Phi_{asy}(x))$ with $R(\Phi_i(x, Q^2))$ (i=CLEO, CZ, BF, BMS) at c.m. energy $\sqrt{s} = 62.4 GeV$.

y	$\frac{R(\Phi_{CLEO}(x, Q^2))}{R(\Phi_{asy}(x))}$	$\frac{R(\Phi_{CZ}(x, Q^2))}{R(\Phi_{asy}(x))}$	$\frac{R(\Phi_{BF}(x, Q^2))}{R(\Phi_{asy}(x))}$	$\frac{R(\Phi_{BMS}(x, Q^2))}{R(\Phi_{asy}(x))}$
-2.52	7.679	1.398	7.142	2.124
-1.92	0.241	0.226	0.313	3.486
0.78	0.051	0.637	4.367	1.849

TABLE II: The distinction between $R(\Phi_{asy}(x))$ with $R(\Phi_i(x, Q^2))$ (i=CLEO, CZ, BF, BMS) at c.m. energy $\sqrt{s} = 62.4 GeV$ and $p_T = 4.9 GeV/c$.

$p_T, GeV/c$	$\frac{R(\Phi_{CLEO}(x, Q^2))}{R(\Phi_{asy}(x))}$	$\frac{R(\Phi_{CZ}(x, Q^2))}{R(\Phi_{asy}(x))}$	$\frac{R(\Phi_{BF}(x, Q^2))}{R(\Phi_{asy}(x))}$	$\frac{R(\Phi_{BMS}(x, Q^2))}{R(\Phi_{asy}(x))}$
10	0.706	0.246	0.438	1.825
35	2.746	0.824	2.746	0.684
95	2.021	0.269	0,807	0.342

TABLE III: The distinction between $R(\Phi_{asy}(x))$ with $R(\Phi_i(x, Q^2))$ (i=CLEO, CZ, BF, BMS) at c.m. energy $\sqrt{s} = 200 GeV$.

y	$\frac{r(\Phi_{CLEO}(x, Q^2))}{r(\Phi_{asy}(x))}$	$\frac{r(\Phi_{CZ}(x, Q^2))}{r(\Phi_{asy}(x))}$	$\frac{r(\Phi_{BF}(x, Q^2))}{r(\Phi_{asy}(x))}$	$\frac{R(\Phi_{BMS}(x, Q^2))}{R(\Phi_{asy}(x))}$
-2.52	3.468	0.564	2.121	4.214
-1.92	1.068	0.204	0.267	0.768
0.78	0.328	0.579	3.322	3.021

TABLE IV: The distinction between $R(\Phi_{asy}(x))$ with $R(\Phi_i(x, Q^2))$ (i=CLEO, CZ, BF, BMS) at c.m. energy $\sqrt{s} = 200 \text{ GeV}$ and $p_T = 15.5 \text{ GeV}/c$.

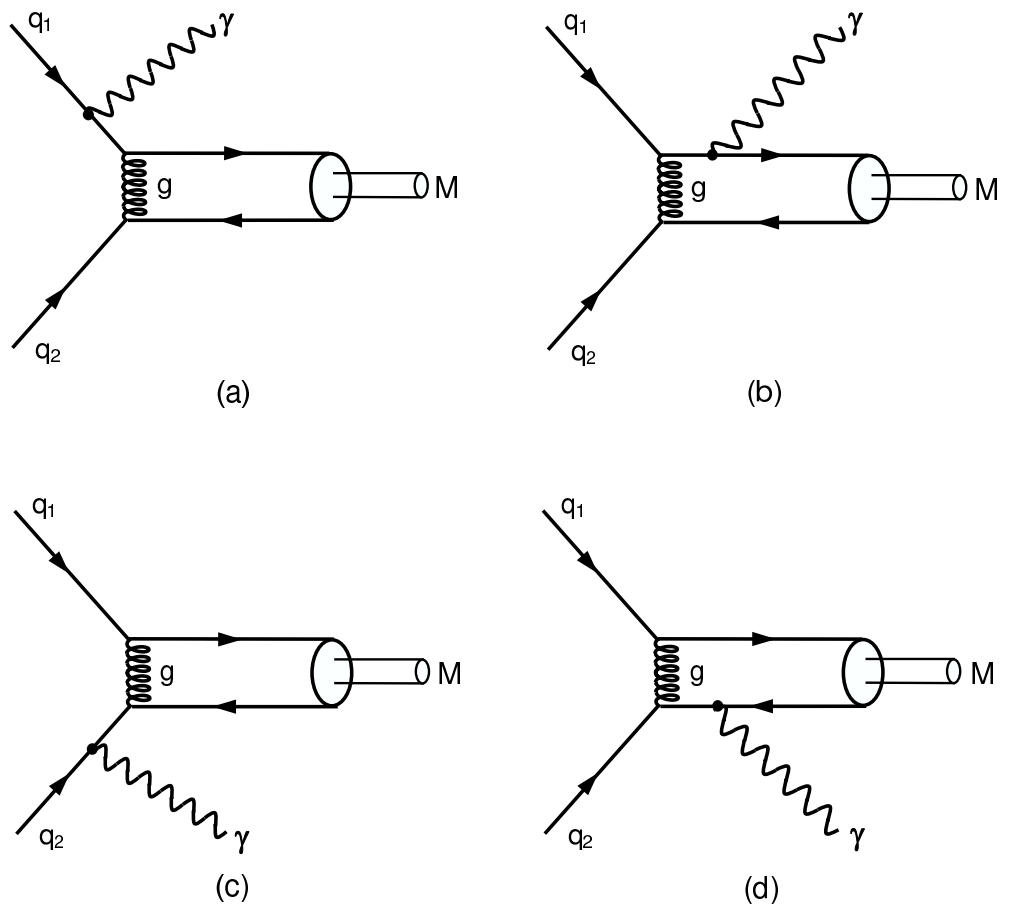


FIG. 1: Feynman diagrams for the higher-twist subprocess, $q_1 q_2 \rightarrow \pi^+ (\text{or } \pi^-) \gamma$.

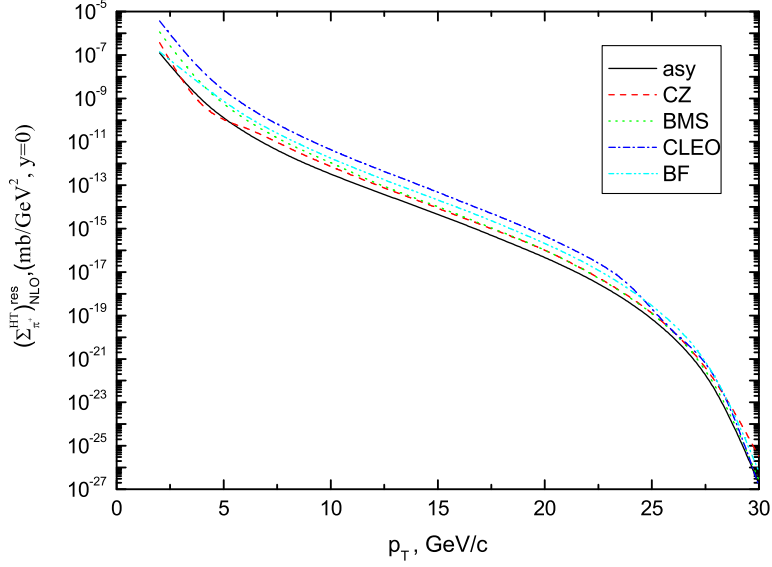


FIG. 2: Next-to-leading order higher-twist π^+ production cross section $(\Sigma_{\pi^+}^{HT})_{NLO}^{res}$ as a function of the p_T transverse momentum of the pion at the c.m.energy $\sqrt{s} = 62.4 \text{ GeV}$.

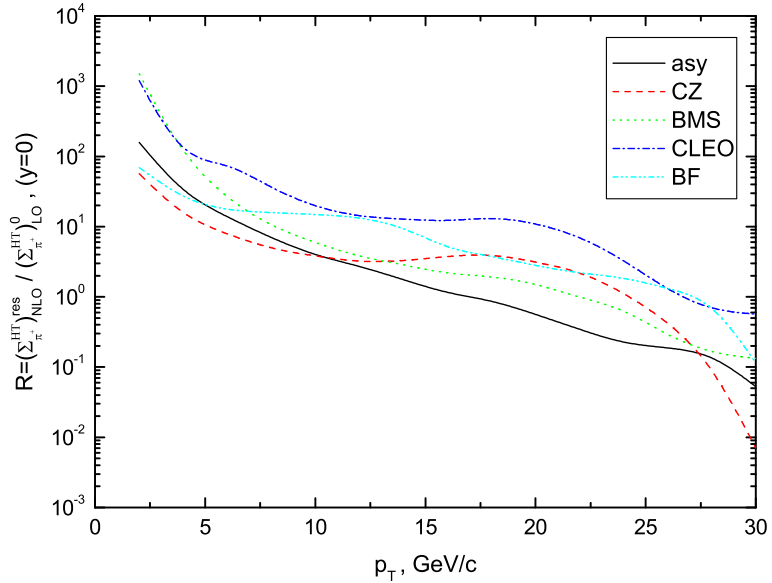


FIG. 3: Ratio $R = (\Sigma_{\pi^+}^{HT})_{NLO}^{res} / (\Sigma_{\pi^+}^{HT})_{LO}^0$, where LO and NLO higher-twist contribution are calculated for the pion rapidity $y = 0$ at the c.m.energy $\sqrt{s} = 62.4 \text{ GeV}$ as a function of the pion transverse momentum, p_T .

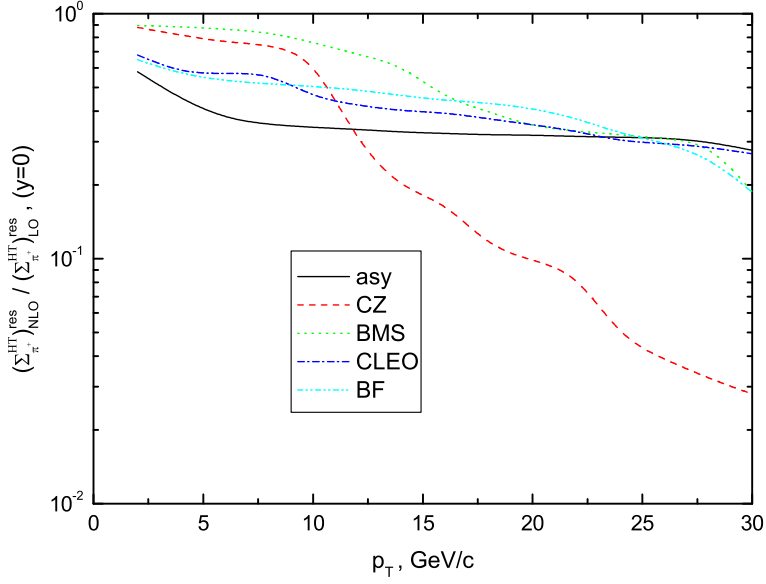


FIG. 4: Ratio $(\Sigma_{\pi^+}^{HT})_{NLO}^{res}/(\Sigma_{\pi^+}^{HT})_{LO}^{res}$, where higher-twist contribution are calculated for the pion rapidity $y = 0$ at the c.m.energy $\sqrt{s} = 62.4 \text{ GeV}$ as a function of the pion transverse momentum, p_T .

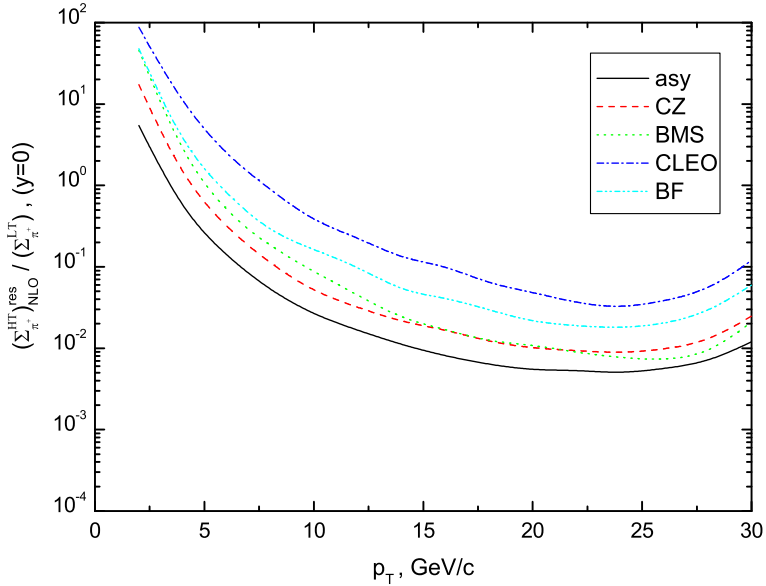


FIG. 5: Ratio $(\Sigma_{\pi^+}^{HT})_{NLO}^{res}/(\Sigma_{\pi^+}^{LT})$, as a function of the p_T transverse momentum of the pion at the c.m.energy $\sqrt{s} = 62.4 \text{ GeV}$.

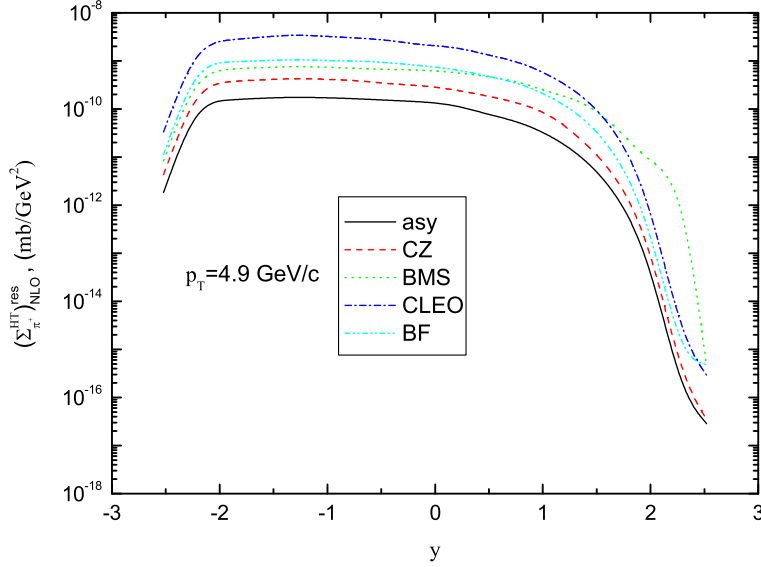


FIG. 6: Next-to-leading order higher-twist π^+ production cross section $(\Sigma_{\pi^+}^{HT})_{NLO}^{res}$, as a function of the y rapidity of the pion at the transverse momentum of the pion $p_T = 4.9 \text{ GeV}/c$, at the c.m. energy $\sqrt{s} = 62.4 \text{ GeV}$.

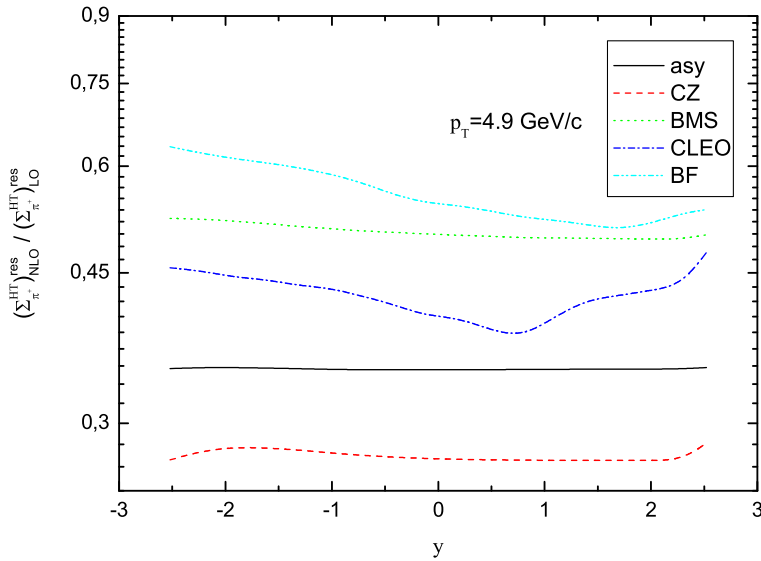


FIG. 7: Ratio $(\Sigma_{\pi^+}^{HT})_{NLO}^{res}/(\Sigma_{\pi^+}^{HT})_{LO}^{res}$, as a function of the y rapidity of the pion at the transverse momentum of the pion $p_T = 4.9 \text{ GeV}/c$, at the c.m. energy $\sqrt{s} = 62.4 \text{ GeV}$.

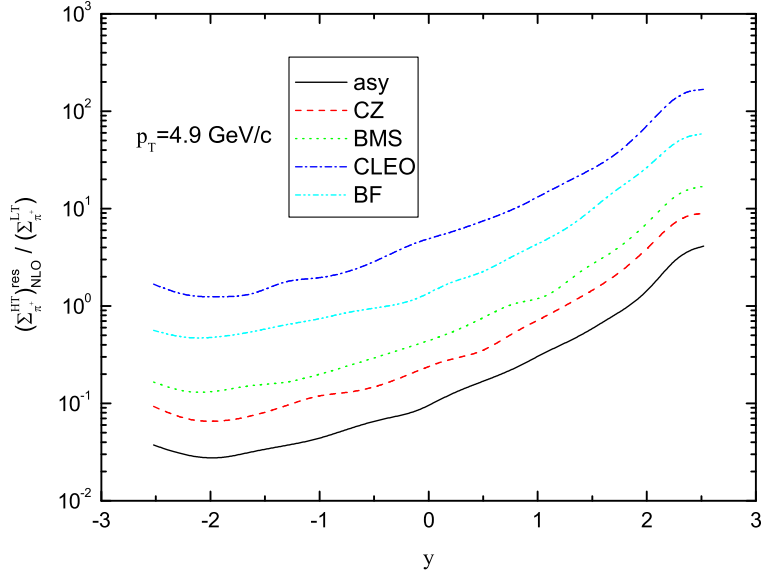


FIG. 8: Ratio $(\Sigma_{\pi^+}^{HT})_{NLO}^{res}/(\Sigma_{\pi^+}^{LT})$, as a function of the y rapidity of the pion at the transverse momentum of the pion $p_T = 4.9 \text{ GeV}/c$, at the c.m. energy $\sqrt{s} = 62.4 \text{ GeV}$.

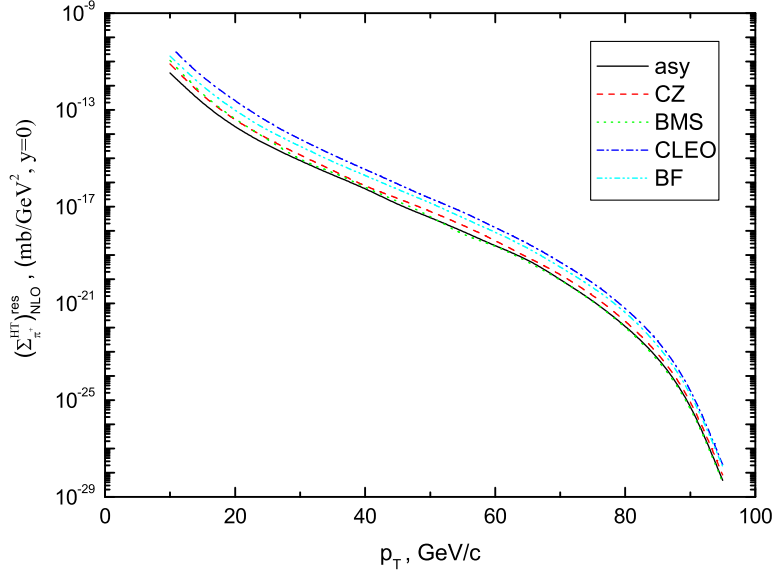


FIG. 9: Next-to-leading order higher-twist π^+ production cross section $(\Sigma_{\pi^+}^{HT})_{NLO}^{res}$ as a function of the p_T transverse momentum of the pion at the c.m.energy $\sqrt{s} = 200 \text{ GeV}$.

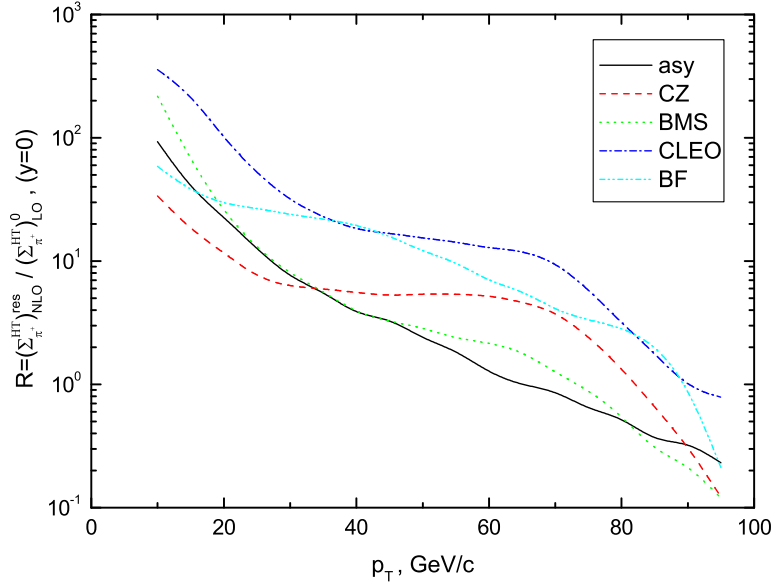


FIG. 10: Ratio $R = (\Sigma_{\pi^+}^{HT})_{NLO}^{res} / (\Sigma_{\pi^+}^{HT})_{LO}^0$, where LO and NLO higher-twist contribution are calculated for the pion rapidity $y = 0$ at the c.m.energy $\sqrt{s} = 200 \text{ GeV}$ as a function of the pion transverse momentum, p_T .

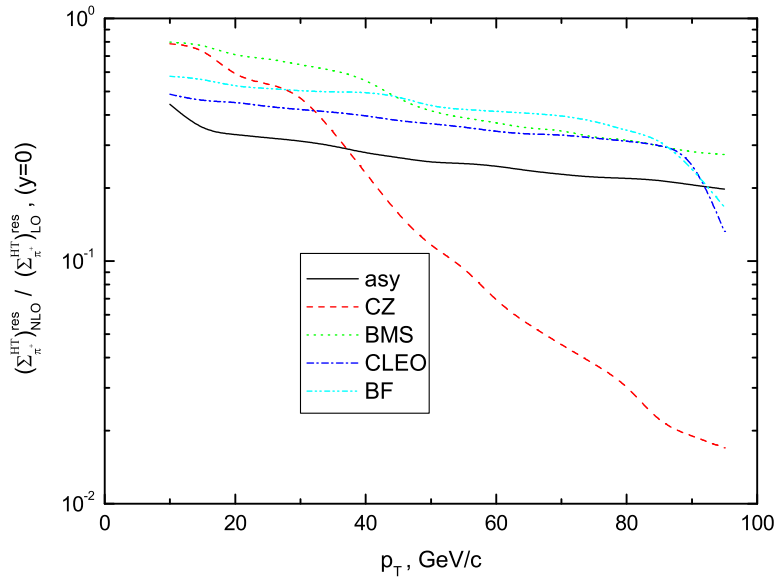


FIG. 11: Ratio $(\Sigma_{\pi^+}^{HT})_{NLO}^{res} / (\Sigma_{\pi^+}^{HT})_{LO}^{res}$, where higher-twist contribution are calculated for the pion rapidity $y = 0$ at the c.m.energy $\sqrt{s} = 200 \text{ GeV}$ as a function of the pion transverse momentum, p_T .

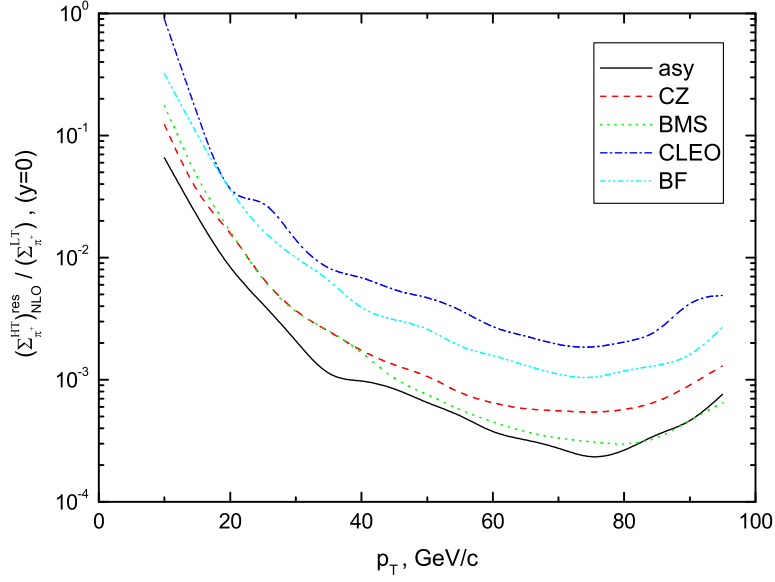


FIG. 12: Ratio $(\Sigma_{\pi^+}^{HT})_{NLO}^{res}/(\Sigma_{\pi^+}^{LT})$, as a function of the p_T transverse momentum of the pion at the c.m.energy $\sqrt{s} = 200 \text{ GeV}$.

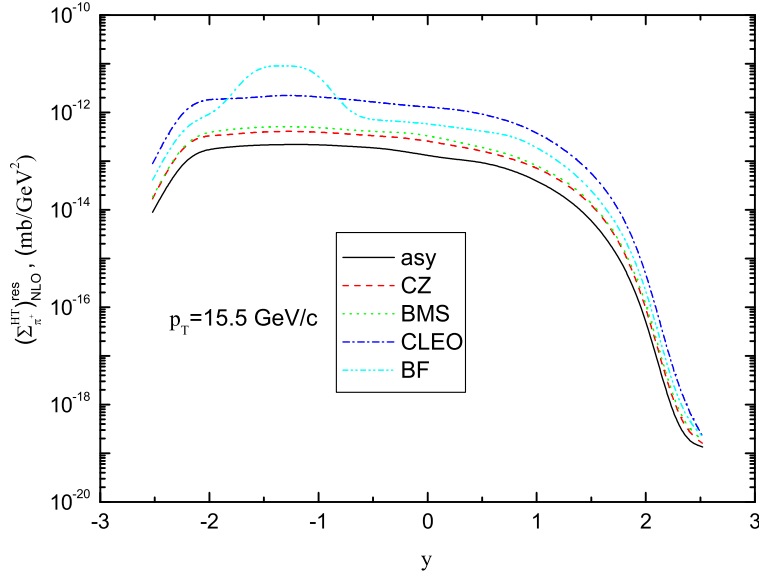


FIG. 13: Next-to-leading order higher-twist π^+ production cross section $(\Sigma_{\pi^+}^{HT})_{NLO}^{res}$, as a function of the y rapidity of the pion at the transverse momentum of the pion $p_T = 15.5 \text{ GeV}/c$, at the c.m. energy $\sqrt{s} = 200 \text{ GeV}$.

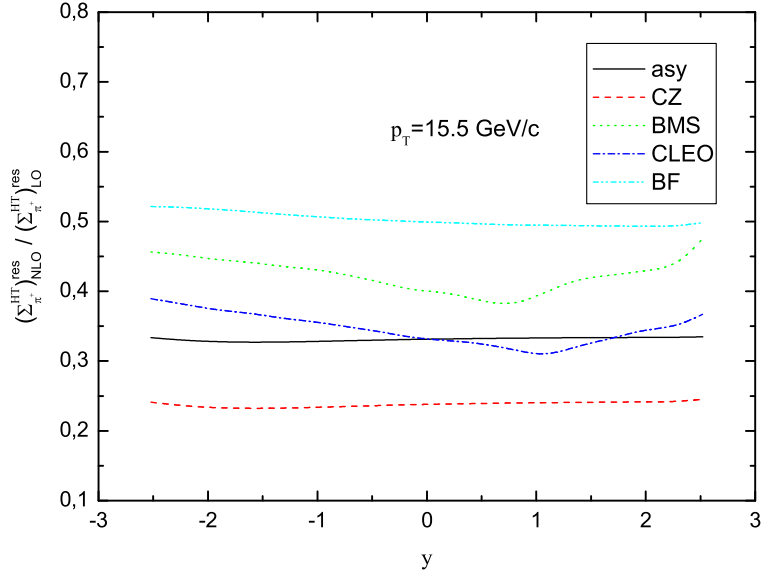


FIG. 14: Ratio $(\Sigma_{\pi^+}^{HT})_{NLO}^{res}/(\Sigma_{\pi^+}^{HT})_{LO}^{res}$, as a function of the y rapidity of the pion at the transverse momentum of the pion $p_T = 15.5 \text{ GeV}/c$, at the c.m. energy $\sqrt{s} = 200 \text{ GeV}$.

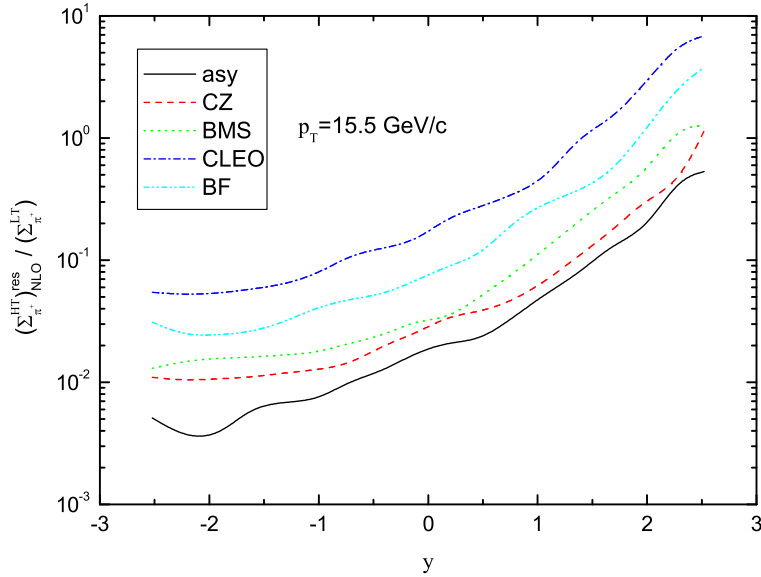


FIG. 15: Ratio $(\Sigma_{\pi^+}^{HT})_{NLO}^{res}/(\Sigma_{\pi^+}^{LT})$, as a function of the y rapidity of the pion at the transverse momentum of the pion $p_T = 15.5 \text{ GeV}/c$, at the c.m. energy $\sqrt{s} = 200 \text{ GeV}$.